Nanoscale Advances

ROYAL SOCIETY OF CHEMISTRY

PAPER

View Article Online
View Journal | View Issue

Cite this: *Nanoscale Adv.*, 2025, **7**, 6620

Optical phonon confinement significantly lowers the hot electron energy loss rate in III-nitride (InN, GaN, and AlN) and GaAs nanoscale structures

Huynh Thi Phuong Thuy[a] and Nguyen Dinh Hien *[bc]

Received 15th May 2025
Accepted 12th August 2025

DOI: 10.1039/d5na00483g

rsc.li/nanoscale-advances

This investigation presents a detailed comparative analysis of the energy loss rate (ELR) in the III-nitride (InN, AlN, and GaN) and GaAs quantum well (QW) heterostructures of hot electrons because of confined and bulk optical phonon (OP) scattering based on the electronic temperature model. This analysis is conducted because of the impact of a quantizing magnetic field and utilizes the framework of OP confinement proposed by Huang and Zhu. The following results are what we have obtained: firstly, the explicit expression of the average ELR in the III-nitride (InN, AlN, and GaN) and GaAs QW heterostructures of hot electrons because of confined OP interaction. Secondly, the graphs describe the dependencies of the ELR in the InN, GaN, and AlN, and GaAs QW heterostructures of hot electrons on the quantizing magnetic field, two-dimensional electronic concentration, temperature of the two-dimensional electrons, and QW heterostructure width for both the aforementioned OP types. Thirdly, the comparative graphs of the above dependencies between the InN, AlN, and GaN, and GaAs material QW heterostructures in all three cases of OPs, including bulk, confinement, and both bulk and confinement are presented. Finally, the various contributions from individual phonon modes to the ELR in the III-nitride (InN, AlN, and GaN) and GaAs QW heterostructures of hot electrons are analyzed. Our research offers insightful knowledge that will support the development and manufacturing of optoelectronic devices.

1 Introduction

Research on the hot electron ELR in low-dimensional systems has recently gained much interest.[1–8] These investigations have offered a perspective on the thermal interactions between phonons and electrons in such low-dimensional systems. It is widely recognized that the energy transfer capabilities of hot electrons have valuable applications in various devices, including calorimeters and detectors, and induce a photoresponse in materials with a monolayer structure.[9] Furthermore, cooling hot electrons is an essential and fundamental aspect of contemporary optoelectronic devices. Consequently, it is essential to comprehend how hot electrons are transported in low-dimensional systems. The energy loss rate in low dimensional systems refers to the rate at which an excited electron loses its energy through various relaxation processes. In low-dimensional systems, where charge carriers are confined in one, two, or three dimensions, the energy loss rate is crucial for understanding the dynamics of carriers, particularly in optoelectronic devices like lasers, photodetectors, and light-emitting diodes.[10] Understanding the mechanisms underlying energy loss is crucial for technological reasons because the majority of semiconductor devices function in high-field environments. In an electric field that is strong, the temperature of the electron gas rises above the surrounding lattice temperature. The emission of various phonon types, depending on the temperature region, results in the electron and lattice reaching equilibrium. Therefore, the investigation of the hot electron ELR (or cooling power) can be utilised as a probe to further study the electron interacting mechanisms with phonons. Additionally, this interaction determines the magnetoconductivity, dynamics of nonequilibrium electrophonon systems, electrons' high-field saturation velocity and low-field mobility at room temperature, and a variety of other phenomena in semiconductor nanostructures, which in turn determine the properties of ultrasmall, high-speed devices.[6] III–V semiconductors have some great optical and electrical features. They have a direct band gap, which means they can efficiently release energy as light, and they also offer low effective mass and high electron mobility, making them useful for various applications.[11] As a result, in the last few years, III–V compound nanostructures have garnered immense attention because of their promising applications in areas such as waveguide devices, photodetection, photovoltaics, and biosensing. This unique category of III–V nanostructures has profoundly transformed the

[a]*Thu Dau Mot University, Ho Chi Minh City, Vietnam. E-mail: thuyhtp@tdmu.edu.vn*
[b]*Institute of Research and Development, Duy Tan University, Da Nang, Vietnam. E-mail: nguyendinhhien2@duytan.edu.vn*
[c]*School of Engineering & Technology, Duy Tan University, Da Nang, Vietnam*

lighting sector due to the high brightness, versatility, and laser diodes (LDs), leading to unprecedented levels of cost and energy savings.[12–14] Specifically, the operational wavelengths of different devices made from III-nitride semiconductors cover the near-infrared to deep-ultraviolet spectrum, as the bandgap can be tuned between 0.7 eV and 6.2 eV.[15] The broad direct band-gap range of III-nitrides is an essential feature for their photonic device applications. This trait allows for effective photon emission and absorption without needing phonon interaction, which is vital for the functionality of these devices, as demonstrated by C. X. Ren.[16] In the last decade, nitride-based semiconductor heterostructures have captured significant attention due to their exciting potential in various cutting-edge fields. From spintronics and high-temperature microwave devices to high-power electronics and optoelectronics, these materials are paving the way for innovations that could transform technology as we know it.[17] Achieving optimal device performance requires a comprehensive understanding of basic electron characteristics as well as a thorough investigation of electron–phonon interaction processes. This knowledge is critical to advancing our capabilities in this field. A deeper comprehension of the interaction of e–p is offered by the hot-electron ELR, as opposed to conventional mobility research. The III-nitride semiconductors, including materials like indium nitride (InN), aluminum nitride (AlN), and gallium nitride (GaN), are important components in the technology that powers light-emitting gadgets like LEDs and lasers. The ability of LEDs with III-nitride materials to emit light effectively and intensely in the blue to UV spectral range represents a breakthrough in technology for lighting. Without these qualities, creating LEDs with white light would be quite difficult.[16] InN, GaN, and AlN, and their respective alloys constitute a category of materials referred to as III-nitrides. This III-nitride semiconductor group is crucial for facilitating compact and efficient high-power applications. These materials help produce light in both the ultraviolet spectrum and visible range, which is useful for various applications. Additionally, they are becoming more popular in power electronics and advanced types of transistors, known as transistors with high-electron-mobility, which are essential for efficient electronic devices.[18–20] Transition metal dopants in GaN and AlN are being explored for their potential applications in spintronics and as spin qubits in quantum information technology. Their unique electronic and magnetic properties may enable advancements in both fields, facilitating the development of novel devices that leverage spin degrees of freedom for enhanced performance and functionalities.[21] In addition, the III-nitrides (InN, GaN, and AlN) continue to emerge as leading contenders for advanced semiconductor device applications. Ongoing advancements in material quality have facilitated the development of various nitride-based devices, including high-efficiency lasers and transistors with high-performance,[22] showcasing their potential in next-generation electronic and optoelectronic systems.[23] To effectively analyze and enhance these devices' design, it is essential to have a comprehensive understanding of electronic transport mechanisms within such materials. To date, investigations have predominantly concentrated on steady-state electronic transport phenomena. Specifically, the velocity-field characteristics of GaN under steady-state conditions have been thoroughly analyzed. In devices with larger dimensions, steady-state electronic transport primarily governs the transport mechanism. Conversely, for smaller-scale devices, it is crucial to also account for transient electron transport effects when assessing overall device performance. Furthermore, Ruch showed that, for GaAs and Si, the average transient electronic velocity can significantly surpass the steady-state drift velocity when optimal electric field conditions are applied.[24] Gallium arsenide (GaAs) nanostructures are increasingly being utilized across various applications within the fields of optoelectronics and semiconductor technology. Their integration is notable in advanced technologies such as thermoelectric devices, tunnel field-effect transistors, solar cells, biosensing platforms, and light-emitting diodes. The unique electronic and optical properties of GaAs at the nanoscale enable enhanced performance and efficiency in these critical applications.[25,26] Several studies have explored hot electron ELR in nanostructures under quantized magnetic fields within the existing literature.[4–7,27] Nonetheless, these studies primarily concentrate on the GaAs material, and they have not thoroughly examined the effects of surface electronic concentration and the thickness of nanoscale structures on hot electron ELR. In particular, confined OP impaction on hot electron ELR compared with the bulk one has not yet been taken into account in these studies. Meanwhile, interactions between electrons and phonons in semiconductor nanostructures influence the acoustic characteristic and mechanical characteristic of such quantum-structures as well as the ultrasensitive detectors' performance limits. The eigenstates of phonons in these nanoscale structures undergo significant modifications due to quantum size effects, leading to substantial alterations in electron transport characteristics compared to bulk materials. Consequently, taking into account the OP confinement is crucial for elucidating electron transport mechanisms within such nanoscale structures.[28] Conversely, the majority of the theories discussed up to this point have overlooked the concept of phonon confinement, addressing the effects of confinement only in specific instances. As is well known, transitions of electrons aided by OPs are crucial in innovative intersubband lasers that function at mid-infrared wavelengths, as the rates of these transitions are crucial for developing and maintaining population inversion necessary for device functionality. These lasers feature narrow nanoscale structures requiring thicknesses as thin as 3 nm to 5 nm. In these configurations, electronic transitions between sub-bands driven by interactions between OPs and electrons serve as the primary relaxation mechanism when the energy difference between the lasing states approaches one unit or an integer multiple of the energy of longitudinal optical (LO) phonon of the bulk semiconductors.[29] Attaining effective phonon confinement and quantization of the spectrum is crucial for regulating phonon transport, such as in phonon engineering, which could pave the way for applications in nanoscale devices.[30] Some advancements have been made in this area, leading to reports on the production and analysis of free-standing, or almost free-standing, quantum dots, wires, and

wells. It is widely recognized that quantum wells alter the configuration and energies of modes of OPs. The existence of heterointerfaces leads to LO-phonon confinement and also results in localized phonons at the interfaces. As a result, applying the bulk Fröhlich Hamiltonian might produce incorrect estimations of electronic transition rates in these laser structures.[29] The interaction between confined-LO-phonons and electrons in QW heterostructures has been investigated through utilising dielectric continuum models as well as models of microscopic lattice dynamics. Among the distinct macroscopic continuum models frequently used in the literature, one relates to the free ionic slab's slab-modes, while the other pertains to the modeled layered structure's guided modes. These models vary in how they establish boundary conditions for phonons' electrostatic potential or their vibrational amplitudes at the interfaces. As is well known, Huang and Zhu have recently introduced a straightforward model of lattice dynamics to characterize confined OPs in quantum-wells and have provided analytical approximations for this model's outcomes.[31] Among the various OP confinement models, the estimates derived from the Huang and Zhu model align closely with experimental findings.[5,32–35] On the other hand, the importance of incorporating the effects of OP confinement in the quantum wells for the quantum-cascade lasers' active region, which are quantitatively designed, has been clearly shown by Mikhail V. Kisin *et al.*[36] Therefore, based on the above reasons, a study of the hot-electron ELR in III-nitride-based semiconductor heterostructures, taking into account the confinement of LO-phonons by applying the Huang and Zhu model, is very necessary. As a result, our findings in this investigation are expected to offer valuable insights into the nanoscale realm for optoelectronic device development, since III-nitride-based QW heterostructures (InN, GaN, and AlN) and GaAs are commonly utilized in the fabrication of optoelectronic devices.

This investigation presents a comparative analysis of the hot-electron ELR resulting from the scattering of confined and bulk OPs with electrons in the InN, GaN, and AlN (III-nitride) and GaAs quantum well heterostructures. This analysis is conducted because of the impact of a quantizing magnetic field and utilises the framework of electronic temperature. Section 2 describes the theoretical framework, including OP and electron confinement models in quantum wells and the model of electronic temperature. Section 3 presents analytical calculation outcomes, focusing on the Hamiltonian of the confined OP-electron interaction in the QW heterostructure semiconductors and the average ELR in the InN, GaN, and AlN (III-nitride) and GaAs QW heterostructures of hot electrons due to OP confinement. Section 4 provides numerical findings and a discussion. Ultimately, Section 5 outlines the conclusions.

2 Basic theoretical models

2.1 Quantum-well OP confinement model

Regarding the confinement model of OPs, according to the dielectric continuum approach, which was employed by Huang and Zhu, two physicists, OPs must be regarded as being confined in a semiconductor heterostructure when the scalar potentials of these OPs disappear at the material interfaces. In this case, both of the boundary conditions, which are the lattice dynamics and electromagnetic conditions, are together satisfied by the confinement model of OPs. Following that, along the QW semiconductor heterostructure's growth direction, the confined OP's scalar potential, $\mathcal{F}^{\mathrm{E(O)}}_{\ell,\eta}(z)$, takes the following form under the proposal of Huang and Zhu.[31,37]

For even (E) modes of OPs confinement:

$$\mathcal{F}^{\mathrm{E}}_{\ell,\eta}(z) = \cos\left(\frac{\pi\ell}{L_{\mathrm{W}}}z\right) - (-1)^{\ell/2}, \quad \ell = 2,\ 4,\ 6, \cdots. \tag{1}$$

For odd (O) modes of OPs confinement:

$$\mathcal{F}^{\mathrm{O}}_{\ell,\eta}(z) = \sin\left(\frac{\pi\Psi_{\ell}}{L_{\mathrm{W}}}z\right) + \frac{\phi_{\ell}}{L_{\mathrm{W}}}z, \quad \ell = 3,\ 5,\ 7, \cdots. \tag{2}$$

In this case, the quantity Ψ_{ℓ} represents solutions that are expressed as $\tan(\Psi_{\ell}\pi/2) = \Psi_{\ell}\pi/2$, with Ψ_{ℓ} and ϕ_{ℓ} satisfying the conditions $\ell - 1 < \Psi_{\ell} < \ell$ and $\phi_{\ell} = -2\sin(\Psi_{\ell}\pi/2)$, respectively. Here, η is signified *via* $(-)$ for the confined OP even modes and *via* $(+)$ for the confined OP odd modes, and simultaneously, ℓ signifies the confined OP's quantum-number along the z-axis.

2.2 Quantum-well electron confinement model

To study the hot-electron energy-loss rate induced by OP confinement in a III-nitride-based semiconductor heterostructure, we consider a III-nitride QW with the system's z-direction where the magnetic field **B** is located, and carriers are free to travel in the (x, y)-plane. Additionally, the matching eigenvalue, $\Xi_{n,j}$, and eigenfunction, $\chi_{n,j}$, of the QW electron are the following:[38–41]

$$\chi_{n,j}(x,y,z) = 1/\sqrt{L_y}\Lambda_n(x - x_0)\exp(ik_y y)\lambda_j(z), \tag{3}$$

$$\Xi_{n,j} = (n + 1/2)\hbar\omega_{\mathrm{B}} + j^2\Xi_0, \tag{4}$$

in the two formulas, the cyclotron frequency and radius are expressed as $\omega_{\mathrm{B}} = B|e|/(m^*_{\mathrm{e}}c)$ and $\Re = \{\hbar c/(|e|B)\}^{1/2}$, respectively. The levels of Landau (LLs) are denoted by $n = 0, 1, 2, \cdots$, while the levels of the electric sub-band are denoted by $j = 1, 2, 3, \cdots$. Furthermore, $\Lambda_n(x - x_0)$ $(x_0 = -\Re^2 k_y)$ is the harmonic oscillator function, in which k_y and L_y are the wave vector and normalization length in the y-axis. Besides, the energy in the III-nitride-based QW heterostructure with the well-width L_{W} at the lowest electric sub-band is $\Xi_0 = (\pi\hbar)^2/(2L_{\mathrm{W}}{}^2 m^*_{\mathrm{e}})$. Here, the QW heterostructure with confinement potential $U(z)$ has the form $U(z) = 0$ when $|z| < L_{\mathrm{W}}/2$ and $U(z) = \infty$ when $|z| > L_{\mathrm{W}}/2$.[40,42,43] In such a case, the wave-function, $\lambda_j(z)$, of an electron in the III-nitride-based QW heterostructure's z-axis is expressed as

$$\lambda_j(z) = \sqrt{2/L_{\mathrm{W}}}\sin(j\pi z/L_{\mathrm{W}} + j\pi/2). \tag{5}$$

2.3 Model of electronic temperature

To investigate the OP confinement influence on the ELR in the III-nitride-based QW semiconductor heterostructure of hot-electrons, we utilize the model of electronic temperature.[3,8] Here, the electronic temperature, which is denoted by T_e, in this model is higher than the lattice temperature, which is denoted by T_ℓ, and it is determined *via* the Fermi–Dirac distribution function. In such a case, the average ELR of hot-electrons in the III-nitride-based QW semiconductor heterostructure is denoted by Ω and has the following form:[3,5,8]

$$\Omega_{\eta=\pm}{}^{\ell} = \left\langle \frac{\mathrm{d}\varepsilon}{\mathrm{d}t} \right\rangle = \frac{1}{\mathcal{N}_e} \sum_{\ell} \sum_{\eta=\pm} \sum_{\mathbf{q}_\parallel} \hbar\omega_{\mathrm{LO}}{}^{q_\parallel, q_\ell} \frac{\partial \mathcal{N}_{\mathbf{q}_\parallel, q_\ell}}{\partial t}, \tag{6}$$

where the factor $\mathcal{N}_{\mathbf{q}_\parallel, q_\ell}/\partial t$ takes the form[5]

$$\begin{aligned} \frac{\partial \mathcal{N}_{\mathbf{q}_\parallel, q_\ell}}{\partial t} = & \sum_{\ell} \sum_{\eta=\pm} \sum_{i,f} \mathcal{P}_{\mathrm{em.}}{}^{\eta,\ell} \mathcal{F}(\varepsilon_f, T_e)\left[1 - \mathcal{F}(\varepsilon_i, T_e)\right] \\ & - \mathcal{P}_{\mathrm{ab.}}{}^{\eta,\ell} \mathcal{F}(\varepsilon_i, T_e)\left[1 - \mathcal{F}(\varepsilon_f, T_e)\right] \end{aligned} \tag{7}$$

In eqn (6) and (7), $\mathcal{N}_e$, $\mathcal{N}_{\mathbf{q}_\parallel, q_\ell}$, and $\hbar\omega_{\mathrm{LO}}{}^{q_\parallel, q_\ell}$ signify the number of electrons in the III-nitride-based QW semiconductor heterostructure, Bose distribution function, and energy of the confined OP with $\mathbf{q} = (\mathbf{q}_\parallel,\ q_\ell)$ being the wave-vector. The scattering rate of the electron is confined in the III-nitride-based QW semiconductor heterostructure conditioned by confined OP emission, which is denoted by $\mathcal{P}_{\mathrm{em.}}{}^{\eta,\ell}$, or confined OP absorption, which is denoted by $\mathcal{P}_{\mathrm{am.}}{}^{\eta,\ell}$. The Fermi–Dirac distribution functions are denoted by $\mathcal{F}(\mathcal{E}_i, T_e)$ and $\mathcal{F}(\mathcal{E}_f, T_e)$ corresponding to an electron's initial, i, and final, f, states at temperature T_e. In such a case, the scattering rate of the electron confined in the III-nitride-based QW semiconductor heterostructure is determined by the Fermi golden rule as follows:[5]

$$\mathcal{P}_{\mathrm{em./ab.}}{}^{\eta=\pm,\ell}(i \to f) = \frac{2\pi \left| \left\langle f \left| H_{\mathrm{el\text{-}oph}}^{\mathrm{conf.}} \right| i \right\rangle \right|^2}{\hbar} \delta\left(\varepsilon_f - \varepsilon_i \pm \hbar\omega_{\mathrm{LO}}{}^{q_\parallel, q_\ell}\right), \tag{8}$$

where $H_{\mathrm{el\text{-}oph}}^{\mathrm{conf.}}$ signifies the Hamiltonian of confined OPs interacting with electrons in the III-nitride quantum well heterostructures. The confined OP energy, $\hbar\omega_{\mathrm{LO}}{}^{q_\parallel, q_\ell}$, is determined by the following expression:

$$\hbar\omega_{\mathrm{LO}}{}^{q_\parallel, q_\ell} = \hbar\sqrt{\left(\omega_{\mathrm{LO}}^0\right)^2 - \beta^2\left(q_\parallel{}^2 + q_\ell{}^2\right)}, \tag{9}$$

where β and ω_{LO}^0 are the velocity parameters in InN, GaN, and AlN, and GaAs quantum well heterostructures and bulk LO-phonon frequency, respectively. Simultaneously, their values are presented in Table 1.

Table 1 The calculations utilized physical parameters of III-nitride (InN, AlN, and GaN) and GaAs materials[48–56]

Parameters	GaN	AlN	InN	GaAs
$m_e^*(\times m_0)$	0.22	0.48	0.11	0.067
$\hbar\omega_{\mathrm{LO}}$ (meV)	91.83	113.02	68.0	36.25
ς_s	9.20	8.50	15.3	13.18
ς_∞	5.35	4.77	8.4	10.89
β (m s^{-1})	6560	9060	6240	4730

3 Analytical calculation results

3.1 Confined OP-electron interaction in the III-nitride quantum-well heterostructures

In this investigation, we utilize the model of the electronic temperature to examine the impact of OP confinement on the ELR of hot electrons in the III-nitride-based QW semiconductor heterostructures. Therefore, we concentrate on calculating how the ELR depends on the quantum-well width, quantizing magnetic field in III-nitride semiconductor materials, electronic concentration and temperature, and different contributions of confined OP modes to the ELR of hot electrons. On the other hand, to clarify the impact of OP confinement on the ELR of hot electrons in this III-nitride QW heterostructure, the studied results due to confined OPs have to be compared carefully with bulk OPs. Very recently, we have reported a detailed study of the ELR of quantum-well hot electrons conditioned by bulk OPs in zinc and cadmium compound materials.[44] Thus, we do not represent in the present work the Hamiltonian of bulk OP interaction and corresponding analytical calculation outcomes for bulk OP, only representing numerical calculation outcomes for a novel material (III-nitride semiconductor) in the bulk OP case. In particular, in this research, confined OP modes are carefully calculated. As is well known, in QWs, the spatial confinement of atoms restricts the phonon modes compared to bulk materials. This leads to modifications in the phonon dispersion relations and the density of states. The confined OPs in QWs exhibit discrete energy levels and reduced phase space for scattering, compared to the continuum of modes in bulk materials. In such a case, the Hamiltonian of the confined-OP-electron interaction by the electron according to the Fröhlich interaction is the following:[43,45,46]

$$\begin{aligned} H_{\mathrm{el\text{-}oph}}^{\mathrm{conf.}} = & \left(\frac{\varsigma^* 4\pi e^2 \hbar\omega_{\mathrm{LO}}{}^{q_\parallel, q_\ell}}{\varsigma_0 \Theta}\right)^{1/2} \sum_{\eta=\pm} \sum_{\ell, \mathbf{q}_\parallel} e^{i\mathbf{q}_\parallel \cdot \mathbf{r}_\parallel} \Pi_{\ell,\eta}\left(\mathbf{q}_\parallel\right) \\ & \times \mathcal{F}_{\ell,\eta}^{\mathrm{E(O)}}(z)\left[a_{\eta,\ell}\left(\mathbf{q}_\parallel\right) + a_{\eta,\ell}^{\dagger}\left(-\mathbf{q}_\parallel\right)\right], \end{aligned} \tag{10}$$

here, $\varsigma^* = \varsigma_\infty{}^{-1} - \varsigma_s{}^{-1}$, where ς_∞, ς_s, and ς_0 respectively denote the dielectric constants in the optical, static, and vacuum regimes. In this context, we define the confined OP annihilation operator as $a_{\eta,\ell}(\mathbf{q}_\parallel)$ and the corresponding confined OP creation operator as $a_{\eta,\ell}^{\dagger}(-\mathbf{q}_\parallel)$. Here, $\mathbf{q}_\parallel = (q_x, q_y)$ represents the confined OP wave vector in the in-plane direction, while $\mathbf{r}_\parallel = (x, y)$ denotes the position vector in the same plane. Additionally, the quantities $\hbar\omega_{\mathrm{LO}}{}^{q_\parallel, q_\ell}$, Θ, and e have been respectively assigned to the longitudinal optical (LO) phonon's energy, system volume, and electronic charge. The expression $\mathcal{F}_{\ell,\eta}^{\mathrm{E(O)}}(z)$ signifies the scalar potential associated with the OP mode. Simultaneously, $\Pi_{\ell,\eta}(\mathbf{q}_\parallel)$ signifies the Fourier coefficient that reflects electron interaction with the confined OP mode, defined by the scalar potential $\mathcal{F}_{\ell,\eta}^{\mathrm{E(O)}}(z)$ in eqn (1) and (2).

In addition, the Fourier coefficient, $\Pi_{\ell,\eta}(\mathbf{q}_\parallel)$, in formula (10) for confined OP-confined-electron interaction in the III-nitride QW heterostructure, is expressed as

$$\Pi_{\ell,\eta}^{\mathrm{E(O)}}\left(q_\parallel\right) = \left\{\frac{2}{L_\mathrm{W}}\int_{-L_\mathrm{W}/2}^{L_\mathrm{W}/2}\times\left[{q_\parallel}^2\left(\mathcal{F}_{\ell,\eta}^{\mathrm{E(O)}}(z)\right)^2+\left(\frac{\mathrm{d}\mathcal{F}_{\ell,\eta}^{\mathrm{E(O)}}(z)}{\mathrm{d}z}\right)^2\right]\mathrm{d}z\right\}^{-1/2} \tag{11}$$

Then, we continued to execute detailed calculations to evaluate this Fourier coefficient as follows:

We set

$$\Pi_1^{\mathrm{E(O)}}\left(q_\parallel\right) = \frac{2}{L_\mathrm{W}}\int_{-L_\mathrm{W}/2}^{L_\mathrm{W}/2}{q_\parallel}^2\left(\mathcal{F}_{\ell,\eta}^{\mathrm{E(O)}}(z)\right)^2\mathrm{d}z \tag{12}$$

and

$$\Pi_2^{\mathrm{E(O)}}\left(q_\parallel\right) = \frac{2}{L_\mathrm{W}}\int_{-L_\mathrm{W}/2}^{L_\mathrm{W}/2}\left(\frac{\mathrm{d}\mathcal{F}_{\ell,\eta}^{\mathrm{E(O)}}(z)}{\mathrm{d}z}\right)^2\mathrm{d}z. \tag{13}$$

Inserting eqn (1) into eqn (12) and (13), for the case of the confined OP even modes ($\ell = 2,\ 4,\ 6,\cdots$) in III-nitride QW heterostructures, we have

$$\begin{aligned}\Pi_1^{\mathrm{E}}\left(q_\parallel\right) &= \frac{2}{L_\mathrm{W}}\int_{-L_\mathrm{W}/2}^{L_\mathrm{W}/2}{q_\parallel}^2\left(\mathcal{F}_{\ell,\eta}^{\mathrm{E}}(z)\right)^2\mathrm{d}z\\ &= \frac{2{q_\parallel}^2}{L_\mathrm{W}}\int_{-L_\mathrm{W}/2}^{L_\mathrm{W}/2}\left[\cos^2\left(\frac{\ell\pi z}{L_\mathrm{W}}\right)-2(-1)^{\ell/2}\cos\left(\frac{\ell\pi z}{L_\mathrm{W}}\right)+(-1)^\ell\right]\mathrm{d}z\\ &= \frac{2{q_\parallel}^2}{L_\mathrm{W}}\int_{-L_\mathrm{W}/2}^{L_\mathrm{W}/2}\left[\frac{1+\cos\left(\frac{2\ell\pi z}{L_\mathrm{W}}\right)}{2}-2(-1)^{\ell/2}\cos\left(\frac{\ell\pi z}{L_\mathrm{W}}\right)+(-1)^\ell\right]\mathrm{d}z\\ &= \frac{2{q_\parallel}^2}{L_\mathrm{W}}\left[\frac{L_\mathrm{W}}{2}+\frac{L_\mathrm{W}}{2\ell\pi}\sin(\ell\pi)-4(-1)^{\ell/2}\frac{L_\mathrm{W}}{\ell\pi}\sin\left(\frac{\ell\pi}{2}\right)+(-1)^\ell L_\mathrm{W}\right]\\ &= 3{q_\parallel}^2\end{aligned} \tag{14}$$

and

$$\begin{aligned}\Pi_2^{\mathrm{E}}\left(q_\parallel\right) &= \frac{2}{L_\mathrm{W}}\int_{-L_\mathrm{W}/2}^{L_\mathrm{W}/2}\left(\frac{\mathrm{d}\mathcal{F}_{\ell,\eta}^{\mathrm{E}}(z)}{\mathrm{d}z}\right)^2\mathrm{d}z\\ &= \frac{2\ell^2\pi^2}{{L_\mathrm{W}}^3}\int_{-L_\mathrm{W}/2}^{L_\mathrm{W}/2}\sin^2\left(\frac{\ell\pi z}{L_\mathrm{W}}\right)\mathrm{d}z\\ &= \frac{\ell^2\pi^2}{{L_\mathrm{W}}^3}\int_{-L_\mathrm{W}/2}^{L_\mathrm{W}/2}\left[1-\cos\left(\frac{2\ell\pi z}{L_\mathrm{W}}\right)\right]\mathrm{d}z\\ &= \frac{\ell^2\pi^2}{{L_\mathrm{W}}^3}\left[L_\mathrm{W}-\frac{L_\mathrm{W}}{\ell\pi}\sin(\ell\pi)\right] = \frac{\ell^2\pi^2}{{L_\mathrm{W}}^2}.\end{aligned} \tag{15}$$

By using the results in eqn (14) and (15), and utilizing the relationship between eqn (11)–(13), we finally obtain $\Pi_{\ell,\eta}^{\mathrm{E}}(q_\parallel)$ for the case of $\eta = (-)$ and $\ell = 2,\ 4,\ 6,\cdots$ as the following expression:

$$\begin{aligned}\Pi_{\ell,\eta}^{\mathrm{E}}\left(q_\parallel\right) &= \left[\Pi_1^{\mathrm{E}}\left(q_\parallel\right)+\Pi_2^{\mathrm{E}}\left(q_\parallel\right)\right]^{-1/2}\\ &= \left[3{q_\parallel}^2+\ell^2\pi^2\Big/{L_\mathrm{W}}^2\right]^{-1/2}.\end{aligned} \tag{16}$$

Inserting eqn (2) into eqn (12) and (13), for the case of the confined OP odd modes ($\ell = 3,\ 5,\ 7,\cdots$), we have $\Pi_1^{\mathrm{O}}(q_\parallel)$, which takes the form:

$$\begin{aligned}\Pi_1^{\mathrm{O}}\left(q_\parallel\right) &= \frac{2}{L_\mathrm{W}}\int_{-L_\mathrm{W}/2}^{L_\mathrm{W}/2}{q_\parallel}^2\left(\mathcal{F}_{\ell,\eta}^{\mathrm{O}}(z)\right)^2\mathrm{d}z\\ &= \frac{2{q_\parallel}^2}{L_\mathrm{W}}\int_{-L_\mathrm{W}/2}^{L_\mathrm{W}/2}\left[\sin^2\left(\frac{\Psi_\ell\pi z}{L_\mathrm{W}}\right)+2\sin\left(\frac{\Psi_\ell\pi z}{L_\mathrm{W}}\right)\frac{\phi_\ell z}{L_\mathrm{W}}+\frac{{\phi_\ell}^2z^2}{{L_\mathrm{W}}^2}\right]\mathrm{d}z\\ &= \frac{2{q_\parallel}^2}{L_W}\int_{-L_\mathrm{W}/2}^{L_\mathrm{W}/2}\left[\frac{1}{2}-\frac{1}{2}\cos\left(\frac{2\Psi_\ell\pi z}{L_\mathrm{W}}\right)+\frac{2\phi_\ell}{L_\mathrm{W}}z\sin\left(\frac{\Psi_\ell\pi z}{L_\mathrm{W}}\right)+\frac{{\phi_\ell}^2z^2}{{L_\mathrm{W}}^2}\right]\mathrm{d}z,\\ &= \frac{2{q_\parallel}^2}{L_\mathrm{W}}\int_{-L_\mathrm{W}/2}^{L_\mathrm{W}/2}\left[\frac{1}{2}-\frac{1}{2}\cos\left(\frac{2\Psi_\ell\pi z}{L_\mathrm{W}}\right)+\frac{{\phi_\ell}^2z^2}{{L_\mathrm{W}}^2}\mathrm{d}z\right],\\ &\quad+\frac{2{q_\parallel}^2}{L_\mathrm{W}}\int_{-L_\mathrm{W}/2}^{L_\mathrm{W}/2}\frac{2\phi_\ell}{L_\mathrm{W}}z\sin\left(\frac{\Psi_\ell\pi z}{L_\mathrm{W}}\right)\mathrm{d}z.\end{aligned} \tag{17}$$

To continue calculating the integral above, we use the value of the following integral:[47]

$$\int y\sin(by)\mathrm{d}y = \frac{\sin(by)}{b^2}-\frac{y\cos(by)}{b} \tag{18}$$

to evaluate the third term of the integral in eqn (24), which takes the form

$$I = \int_{-L_\mathrm{W}/2}^{L_\mathrm{W}/2}\frac{2\phi_\ell}{L_\mathrm{W}}z\sin\left(\frac{\Psi_\ell\pi z}{L_\mathrm{W}}\right)\mathrm{d}z, \tag{19}$$

and simultaneously use the conditions of the quantities Ψ_ℓ and ϕ_ℓ given by the following equations:

$$\phi_\ell = -2\sin(\Psi_\ell\pi/2) \tag{20}$$

and

$$\tan(\Psi_\ell\pi/2) = \Psi_\ell\pi/2, \tag{21}$$

simultaneously, applying eqn (20) and (21), we have

$$\cos(\Psi_\ell\pi/2) = -\phi_\ell/(\pi\Psi_\ell). \tag{22}$$

Following the systematic calculations, we were able to obtain the following result:

$$\sin(\pi\Psi_\ell) = {\phi_\ell}^2/(\pi\Psi_\ell). \tag{23}$$

Using the results in eqn (18), (22), and (23) for eqn (24), we finally obtain

$$\Pi_1^{\mathrm{O}}\left(q_\parallel\right) = {q_\parallel}^2\left[1+{\phi_\ell}^2\left(\frac{1}{6}-\frac{1}{\pi^2{\Psi_\ell}^2}\right)\right]. \tag{24}$$

$$\begin{aligned}\Pi_2^{\mathrm{O}}\left(q_{\parallel}\right) &= \frac{2}{L_{\mathrm{W}}}\int_{-L_{\mathrm{W}}/2}^{L_{\mathrm{W}}/2}\left(\frac{\mathrm{d}\mathcal{F}_{\ell,\eta}^{\mathrm{O}}(z)}{\mathrm{d}z}\right)^2\mathrm{d}z \\ &= \frac{2}{L_{\mathrm{W}}}\int_{-L_{\mathrm{W}}/2}^{L_{\mathrm{W}}/2}\left[\frac{{\Psi_\ell}^2\pi^2}{{L_{\mathrm{W}}}^2}\cos^2\left(\frac{\Psi_\ell\pi z}{L_{\mathrm{W}}}\right)+\frac{2\pi\Psi_\ell\phi_\ell}{{L_{\mathrm{W}}}^2}\cos\left(\frac{\Psi_\ell\pi z}{L_{\mathrm{W}}}\right)+\frac{{\phi_\ell}^2}{{L_{\mathrm{W}}}^2}\right]\mathrm{d}z \\ &= \frac{2}{L_{\mathrm{W}}}\int_{-L_{\mathrm{W}}/2}^{L_{\mathrm{W}}/2}\left[\frac{{\Psi_\ell}^2\pi^2}{{L_{\mathrm{W}}}^2}\frac{\left(1+\cos\left(\frac{2\Psi_\ell\pi z}{L_{\mathrm{W}}}\right)\right)}{2}+\frac{2\pi\Psi_\ell\phi_\ell}{{L_{\mathrm{W}}}^2}\cos\left(\frac{\Psi_\ell\pi z}{L_{\mathrm{W}}}\right)+\frac{{\phi_\ell}^2}{{L_{\mathrm{W}}}^2}\right]\mathrm{d}z \\ &= \frac{1}{L_{\mathrm{W}}}\int_{-L_{\mathrm{W}}/2}^{L_{\mathrm{W}}/2}\left[\frac{{\Psi_\ell}^2\pi^2}{{L_{\mathrm{W}}}^2}+\frac{{\Psi_\ell}^2\pi^2}{{L_{\mathrm{W}}}^2}\cos\left(\frac{2\Psi_\ell\pi z}{L_{\mathrm{W}}}\right)+\frac{4\pi\Psi_\ell\phi_\ell}{{L_{\mathrm{W}}}^2}\cos\left(\frac{\Psi_\ell\pi z}{L_{\mathrm{W}}}\right)+2\frac{{\phi_\ell}^2}{{L_{\mathrm{W}}}^2}\right]\mathrm{d}z \\ &= \frac{{\Psi_\ell}^2\pi^2-{\phi_\ell}^2}{{L_{\mathrm{W}}}^2}.\end{aligned} \tag{25}$$

The expression of $\Pi_2^{\mathrm{O}}(q_{\parallel})$ is calculated as follows:

From the results in eqn (24) and (25), and using eqn (11)–(13), we finally obtain $\Pi_{\ell,\eta}^{\mathrm{O}}(q_{\parallel})$ for the case of $\eta = (+)$ and $\ell = 3,\ 5,\ 7,\cdots$ as follows:

$$\begin{aligned}\Pi_{\ell,\eta}^{\mathrm{O}}\left(q_{\parallel}\right) &= \left[\Pi_1^{\mathrm{O}}\left(q_{\parallel}\right)+\Pi_2^{\mathrm{O}}\left(q_{\parallel}\right)\right]^{-1/2} \\ &= \left\{{q_{\parallel}}^2\left[1+{\phi_\ell}^2\left(\frac{1}{6}-\frac{1}{\pi^2{\Psi_\ell}^2}\right)\right]+\frac{{\Psi_\ell}^2\pi^2-{\phi_\ell}^2}{{L_{\mathrm{W}}}^2}\right\}^{-1/2}.\end{aligned} \tag{26}$$

Following the systematic calculations by using the results in eqn (16) and (26), we were able to obtain the following general result:

$$\Pi_{\ell,\eta}^{\mathrm{E(O)}}\left(q_{\parallel}\right) = 1\Big/\sqrt{\tau_{\ell,\eta}^{\mathrm{E(O)}}{q_{\parallel}}^2+\upsilon_{\ell,\eta}^{\mathrm{E(O)}}\Big/{L_{\mathrm{W}}}^2}, \tag{27}$$

here, the factors $\tau_{\ell,(-)}^{\mathrm{E}}$ and $\upsilon_{\ell,(-)}^{\mathrm{E}}$ are given by

$$\tau_{\ell,(-)}^{\mathrm{E}} = 3 \tag{28}$$

and

$$\upsilon_{\ell,(-)}^{\mathrm{E}} = \ell^2\pi^2 \tag{29}$$

for even confined OP modes ($\ell = 2,\ 4,\ 6,\cdots$), and

$$\tau_{\ell,(+)}^{\mathrm{O}} = 1+{\phi_\ell}^2\left[1/6-1/\left(\pi^2{\Psi_\ell}^2\right)\right] \tag{30}$$

and

$$\upsilon_{\ell,(+)}^{\mathrm{O}} = {\Psi_\ell}^2\pi^2-{\phi_\ell}^2 \tag{31}$$

for odd confined OP modes ($\ell = 3,\ 5,\ 7,\cdots$) in III-nitride based QW semiconductor heterostructures. This result will be used to calculate the average ELR of hot electrons in III-nitride-based QW semiconductor heterostructures because of confined-OP interaction, as shown below.

3.2 Average ELR in the III-nitride quantum-well heterostructures of hot-electrons because of OP confinement

By using the expressions which are given in the model of electronic temperature and the Hamiltonian of the confined-OP-electron interaction as mentioned above and the following systematic calculations, we were able to determine that the average ELR in III-nitride-based QW semiconductor heterostructures of hot-electrons because of confined-OPs has the following form:

$$\begin{aligned}{\Omega_{\eta=\pm}}^{\ell} = {} & \frac{4e^2\left(\hbar{\omega_{\mathrm{LO}}}^{q_{\parallel},q_\ell}\right)^2\mathcal{N}_{\mathbf{q}_{\parallel},q_\ell}}{L_{\mathrm{W}}\mathcal{N}_{\mathrm{e}}\Re^2}\left(\frac{1}{\varsigma_\infty}-\frac{1}{\varsigma_0}\right)\left\{\exp\left(\frac{\vartheta}{T_\ell}-\frac{\vartheta}{T_{\mathrm{e}}}\right)-1\right\} \\ & \times\sum_{j,j'}\sum_{n,n'}f\left(\Xi_{n,j},T_{\mathrm{e}}\right)\left[1-f\left(\Xi_{n,j}+\hbar{\omega_{\mathrm{LO}}}^{q_{\parallel},q_\ell},T_{\mathrm{e}}\right)\right] \\ & \times\sum_{n=1}^{n_1}\left[\frac{2}{\pi}\frac{\Gamma}{\Gamma^2+4\left(\hbar\omega_{\mathrm{c}}-\hbar{\omega_{\mathrm{LO}}}^{q_{\parallel},q_\ell}\right)^2}\times\sum_{\ell=2}^{\ell_1}\left|{\zeta_{j,j'}}^{\ell,\eta,\mathrm{E(O)}}\right|^2\int_0^{\infty}\left|\Pi_{\ell,\eta}\left(q_{\parallel}\right)\right|^2\left|J_{n,n'}\left(q_{\parallel}\right)\right|^2\mathrm{d}q_{\parallel}\right] \\ & \times\delta\left[\left(j'^2-j^2\right)\Xi_0+\left(n'-n\right)\hbar\omega_{\mathrm{c}}-\hbar{\omega_{\mathrm{LO}}}^{q_{\parallel},q_\ell}\right].\end{aligned} \tag{32}$$

Here, $\vartheta = \hbar{\omega_{\mathrm{LO}}}^{q_{\parallel},q_\ell}/k_{\mathrm{B}}$ and $q_\perp = (q_x,\ q_y)$. $\mathcal{N}_{\mathrm{e}}$ and e denote the electronic concentration and charge, respectively, while $\mathcal{N}_{\mathbf{q}_{\parallel},q_\ell}$ denotes the Bose distribution function. The quantity $|J_{n,n'}(q_\perp)|^2$ is expressed as

$$\left|J_{n,n'}(q_\perp)\right|^2 = \frac{\aleph_2!\exp\left[-(\Re q_\perp)^2/2\right]\left[(\Re q_\perp)^2/2\right]^{\aleph_1-\aleph_2}}{\aleph_1!} \times \left[\mathcal{L}_{\aleph_2}^{\aleph_1-\aleph_2}\left[(\Re q_\perp)^2/2\right]\right]^2, \quad (33)$$

with the Laguerre polynomials expressed as $\mathcal{L}_{\aleph_2}^{\aleph_1-\aleph_2}[(\Re q_\perp)^2/2]$ and $\aleph_1 = \max(n', n)$; conversely, $\aleph_2 = \min(n', n)$. The overlap integral, $\zeta_{j,j'}^{\ell,\eta,\mathrm{E(O)}}$, is expressed as

$$\zeta_{j,j'}^{\ell,\eta,\mathrm{E(O)}} = \int_{-L_W/2}^{L_W/2} \lambda_j^*(z)\mathcal{F}_{\ell,\eta}^{\mathrm{E(O)}}(z)\lambda_j(z)\mathrm{d}z. \quad (34)$$

We now perform the evaluation of eqn (34) for intrasubband transitions ($1 \rightarrow 1$) by utilizing the proposal of Huang and Zhu, as is shown in (1) and (2).

Inserting eqn (1) and (5) into eqn (34), for the case of the confined OP even modes ($\ell = 2, 4, 6, \cdots$) in intrasubband transitions, we have

$$\begin{aligned}\zeta_{1,1}^{\ell,\eta,\mathrm{E}} &= \frac{2}{L_W}\int_{-L_W/2}^{L_W/2}\sin^2\left(\frac{\pi z}{L_W}+\frac{\pi}{2}\right)\left[\cos\left(\frac{\ell\pi z}{L_W}\right)-(-1)^{\ell/2}\right]\mathrm{d}z \\ &= \frac{2}{L_W}\int_{-L_W/2}^{L_W/2}\cos^2\left(\frac{\pi z}{L_W}\right)\left[\cos\left(\frac{\ell\pi z}{L_W}\right)-(-1)^{\ell/2}\right]\mathrm{d}z \\ &= \frac{1}{L_W}\int_{-L_W/2}^{L_W/2}\left[1+\cos\left(\frac{2\pi z}{L_W}\right)\right]\left[\cos\left(\frac{\ell\pi z}{L_W}\right)-(-1)^{\ell/2}\right]\mathrm{d}z \\ &= \frac{1}{L_W}\int_{-L_W/2}^{L_W/2}\left[\cos\left(\frac{\ell\pi z}{L_W}\right)-(-1)^{\ell/2}+\cos\left(\frac{2\pi z}{L_W}\right)\cos\left(\frac{\ell\pi z}{L_W}\right)-\cos\left(\frac{2\pi z}{L_W}\right)(-1)^{\ell/2}\right]dz.\end{aligned} \quad (35)$$

Then, we continued to carry out some additional development steps; we have

$$\begin{aligned}\zeta_{1,1}^{\ell,\eta,\mathrm{E}} &= \frac{1}{L_W}\int_{-L_W/2}^{L_W/2}\left\{\cos\left(\frac{\ell\pi z}{L_W}\right)+\frac{1}{2}\left[\cos\left(\frac{(\ell+2)\pi z}{L_W}\right)+\cos\left(\frac{(2-\ell)\pi z}{L_W}\right)\right]-\cos\left(\frac{2\pi z}{L_W}\right)(-1)^{\ell/2}-(-1)^{\ell/2}\right\}\mathrm{d}z \\ &= \frac{1}{L_W}\left\{\frac{L_W}{\ell\pi}2\sin\left(\frac{\ell\pi}{2}\right)-(-1)^{\ell/2}L_W+\frac{1}{2}\left[\frac{L_W}{(\ell+2)\pi}2\sin\left(\frac{(\ell+2)\pi}{2}\right)+\frac{L_W}{(2-\ell)\pi}2\sin\left(\frac{(2-\ell)\pi}{2}\right)\right]-\frac{L_W}{2\pi}2\sin(\pi)(-1)^{\ell/2}\right\} \\ &= \frac{1}{L_W}\left\{\frac{L_W}{\ell\pi}2\sin\left(\frac{\ell\pi}{2}\right)-(-1)^{\ell/2}L_W+\frac{1}{2}\left[\frac{L_W}{(\ell+2)\pi}2\sin\left(\frac{(\ell+2)\pi}{2}\right)+\frac{L_W}{(2-\ell)\pi}2\sin\left(\frac{(2-\ell)\pi}{2}\right)\right]\right\}.\end{aligned} \quad (36)$$

Now, from expression (36), we consider the following two cases for $\ell \neq 2$ and $\ell = 2$:

For the case of $\ell \neq 2$, using (36), we obtain

$$\zeta_{1,1}^{\ell\neq2,\eta,\mathrm{E}} = -(-1)^{\ell/2}. \quad (37)$$

For the case of $\ell = 2$, we have

$$\begin{aligned}\zeta_{1,1}^{\ell=2,\eta,\mathrm{E}} &= \frac{2}{L_W}\int_{-L_W/2}^{L_W/2}\left[-(-1)^{\ell/2}+\cos\left(\frac{\ell\pi z}{L_W}\right)\right]\sin^2\left(\frac{\pi z}{L_W}+\frac{\pi}{2}\right)\mathrm{d}z \\ &= \frac{2}{L_W}\int_{-L_W/2}^{L_W/2}\left[1+\cos\left(\frac{2\pi z}{L_W}\right)\right]\cos^2\left(\frac{\pi z}{L_W}\right)\mathrm{d}z, \\ &= \frac{1}{L_W}\int_{-L_W/2}^{L_W/2}\left[1+\cos\left(\frac{2\pi z}{L_W}\right)\right]\left[\cos\left(\frac{2\pi z}{L_W}\right)+1\right]\mathrm{d}z \\ &= \frac{1}{L_W}\int_{-L_W/2}^{L_W/2}\left[1+2\cos\left(\frac{2\pi z}{L_W}\right)+\cos^2\left(\frac{2\pi z}{L_W}\right)\right]\mathrm{d}z.\end{aligned} \quad (38)$$

We then proceeded to execute a few more development steps; we have

$$\begin{aligned}\zeta_{1,1}^{\ell=2,\eta,\mathrm{E}} &= \frac{1}{L_W}\int_{-L_W/2}^{L_W/2}\left[1+\cos\left(\frac{2\pi z}{L_W}\right)+\frac{1}{2}\left[1+\cos\left(\frac{4\pi z}{L_W}\right)\right]+\cos\left(\frac{2\pi z}{L_W}\right)\mathrm{d}z\right], \\ &= \frac{1}{L_W}\left\{\frac{L_W}{\pi}\sin\pi+L_W+\frac{1}{2}\left[L_W+\frac{L_W}{2\pi}\sin(2\pi)\right]+\frac{L_W}{\pi}\sin\pi\right\} = \frac{3}{2}.\end{aligned} \quad (39)$$

Finally, combining the results in the cases of $\ell = 2$ and $\ell \neq 2$, we obtain

$$\zeta_{1,1}{}^{\ell,\eta,\mathrm{E}} = (-1)^{\ell/2}(\delta_{\ell,2} - 1) + \frac{3}{2}\delta_{\ell,2}, \quad \ell = 2, 4, 6, \cdots. \tag{40}$$

Inserting eqn (2) and (5) into eqn (34), for the case of the confined OP odd modes ($\ell = 3,\ 5,\ 7, \cdots$) in intrasubband transitions, we have

$$\begin{aligned}
\zeta_{1,1}{}^{\ell,\eta,\mathrm{O}} &= \frac{2}{L_\mathrm{W}}\int_{-L_\mathrm{W}/2}^{L_\mathrm{W}/2}\left[\frac{\phi_\ell}{L_\mathrm{W}}z + \sin\left(\frac{\Psi_\ell \pi z}{L_\mathrm{W}}\right)\right]\sin^2\left(\frac{\pi z}{L_\mathrm{W}} + \frac{\pi}{2}\right)\mathrm{d}z \\
&= \frac{2}{L_\mathrm{z}}\int_{-L_\mathrm{W}/2}^{L_\mathrm{W}/2}\left[\frac{\phi_\ell}{L_\mathrm{W}}z + \sin\left(\frac{\Psi_\ell \pi z}{L_\mathrm{W}}\right)\right]\cos^2\left(\frac{\pi z}{L_\mathrm{W}}\right)\mathrm{d}z \\
&= \frac{1}{L_\mathrm{W}}\int_{-L_\mathrm{W}/2}^{L_\mathrm{W}/2}\left[\frac{\phi_\ell}{L_\mathrm{W}}z + \sin\left(\frac{\Psi_\ell \pi z}{L_\mathrm{W}}\right)\right]\left[1 + \cos\left(\frac{2\pi z}{L_W}\right)\right]\mathrm{d}z \\
&= \frac{1}{L_\mathrm{W}}\int_{-L_\mathrm{W}/2}^{L_\mathrm{W}/2}\left[\frac{\phi_\ell}{L_\mathrm{W}}z + \sin\left(\frac{\Psi_\ell \pi z}{L_\mathrm{W}}\right) + \cos\left(\frac{2\pi z}{L_\mathrm{W}}\right)\sin\left(\frac{\Psi_\ell \pi z}{L_\mathrm{W}}\right) + \cos\left(\frac{2\pi z}{L_\mathrm{W}}\right)\frac{\phi_\ell}{L_\mathrm{W}}z\right]\mathrm{d}z.
\end{aligned} \tag{41}$$

After that, we proceeded to perform a few more transform steps; we have

$$\begin{aligned}
\zeta_{1,1}{}^{\ell,\eta,\mathrm{O}} &= \frac{1}{L_\mathrm{W}}\int_{-L_\mathrm{W}/2}^{L_\mathrm{W}/2}\left\{\sin\left(\frac{\Psi_\ell \pi z}{L_\mathrm{W}}\right) + \frac{\phi_\ell}{L_\mathrm{W}}z + \frac{1}{2}\left[\sin\left(\frac{(2+\Psi_\ell)\pi}{L_\mathrm{W}}z\right) + \sin\left(\frac{(\Psi_\ell - 2)\pi}{L_\mathrm{W}}z\right)\right] + \cos\left(\frac{2\pi z}{L_\mathrm{W}}\right)\frac{\phi_\ell}{L_\mathrm{W}}z\right\}\mathrm{d}z, \\
&= \frac{\phi_\ell}{{L_\mathrm{W}}^2}\int_{-L_\mathrm{W}/2}^{L_\mathrm{W}/2} z\cos\left(\frac{2\pi z}{L_\mathrm{W}}\right)\mathrm{d}z = \frac{\phi_\ell}{2\pi L_\mathrm{W}}\int_{-L_\mathrm{W}/2}^{L_\mathrm{W}/2} z\mathrm{d}\left[\sin\left(\frac{2\pi z}{L_\mathrm{W}}\right)\right]\mathrm{d}z = 0.
\end{aligned} \tag{42}$$

Based on the findings, we were able to determine that the intrasubband transition is solely caused by the confined OP even modes.

In addition, in eqn (32) of the average ELR of hot-electrons in III-nitride-based QW semiconductor heterostructures due to confined OPs the integral $\int_0^\infty \left|\Pi_{\ell,\eta}(\mathbf{q}_\parallel)\right|^2\left|J_{n,n'}(q_\perp)\right|^2\mathrm{d}q_\perp$ has to be calculated in detail. Following the systematic calculations, we were able to obtain the following results:

$$\begin{aligned}
\int_0^\infty \left|\Pi_{\ell,\eta}\left(\mathbf{q}_\parallel\right)\right|^2\left|J_{n,n'}(q_\perp)\right|^2\mathrm{d}q_\perp &= \frac{1}{n!}\int_0^\infty \frac{\left(\Re^2{q_\parallel}^2/2\right)^n\exp\left(-\Re^2{q_\parallel}^2/2\right)}{3{q_\parallel}^2 + \left(\ell\pi/L_\mathrm{W}\right)^2}q_\parallel\mathrm{d}q_\parallel \\
&= \frac{1}{2}\exp\left[(\ell\pi\Re)^2/\left(2{L_\mathrm{W}}^2\right)\right]\Xi_{n+1,j}\left[(\ell\pi\Re)^2/\left(2{L_\mathrm{W}}^2\right)\right].
\end{aligned} \tag{43}$$

To demonstrate that in III-nitride-based semiconductor heterostructures, OP confinement dramatically lowers the hot-electron ELR, we need to solve the two following works: firstly, we make the numerical comparative computations between III-nitride QW heterostructures (InN, GaN, and AlN) for both the bulk and confined OP types by using analytical outcomes obtained in Subsection 3. Secondly, we plot the graphs to show the hot-electron energy-loss rate dependence on the confined OP modes, quantising magnetic field, two-dimensional electronic concentration, temperature of the two-dimensional electron, and QW width for both the aforementioned OP types. In particular, to add interest to this research, semiconductor GaAs is also taken into account and compared with III-nitride QW heterostructures, including InN, GaN, and AlN.

4 Numerical results and discussion

In Section 4, through the utilization of analytical results acquired in Section 3, we make the numerical comparative computations related to the average ELR of hot electrons in the InN, GaN, and AlN (III-nitride) and GaAs QW heterostructures due to interactions between confined and bulk OPs with confined electrons. The calculations utilized the physical parameters of InN, GaN, and AlN (III-nitride) QW heterostructures, along with GaAs QW heterostructure, as shown in Table 1. These numerical comparative computations include (i) numerical computations and plotting the comparative graphs

to show the hot-electron ELR dependence on the 2D electronic concentration, temperature of the 2D electron, quantizing magnetic field, and QW width in InN, GaN, and AlN (III-nitride) and GaAs QW heterostructures for both the aforementioned OP types to clarify the significant dissimilarity between III-nitride and GaAs semiconductors and between confined and bulk phonons; (ii) numerical calculations and plotting the comparative graphs to show the hot-electron ELR dependence on the temperature of the 2D electron and QW-width in InN, GaN, and AlN, and GaAs QW heterostructures at different confined OP modes ($m = 2$, 4, 6, 8, 10) to clarify the significant dissimilarity between these confined OP modes in both III-nitride and GaAs QW heterostructures. The detailed outcomes are shown in the following figures.

In Fig. 1, the ELR in the III-nitride and GaAs QW heterostructure of hot electrons because of confined and bulk OP interactions is shown. Specifically, the hot electron ELR is compared between confined and bulk OPs and between InN, GaN, and AlN (III-nitride) and GaAs materials in a QW heterostructure *versus* the quantizing magnetic field B. In this calculation, the confined OP mode $m = 2$, width of QW $L_W = 5$ nm, lattice and electron temperatures $T_\ell = 4.2$ K and $T_e = 300$ K, and electronic concentration $n_e = 10^{16}$ m^{-2} are used. Comprehending the nature of energy transport of hot electrons in III-nitride QW heterostructures is essential. One of the key methods for transferring energy from hot electrons in such heterostructures is by dissipating their energy to phonons. It is widely acknowledged that when a two-dimensional (2D) electron in the InN, GaN, and AlN (III-nitride) and GaAs QW heterostructure is exposed to a quantizing magnetic field, the transition from one Landau level to another occurs by appropriate-energy phonon absorption (emission). A key factor in understanding the cooling process of hot electrons in the III-nitride and GaAs QW heterostructure is the ELR, which typically indicates how quickly electrons lose energy through phonon emission. In the current computation, the maxima in the graphs are associated with the electrons' resonant relaxation in the III-nitride QW heterostructures, such as GaN, AlN, and InN, along with the GaAs QW heterostructure between various inter-Landau levels facilitated through confined OP emission. They happen when $\Delta n\omega_B = \omega_{LO}{}^{q_\parallel, q_\ell}$ $(\Delta n = 1, 2, 3, \cdots)$ or $\Delta n|e|B/(m_e^* c) = \omega_{LO}{}^{q_\parallel, q_\ell}$, the resonance conditions, are satisfied. In this process of magneto-phonon resonance (MPR), the energy difference between the starting and ending states, corresponds to the phonon mode's energy. The corresponding relaxation time in the III-nitride QW heterostructures will

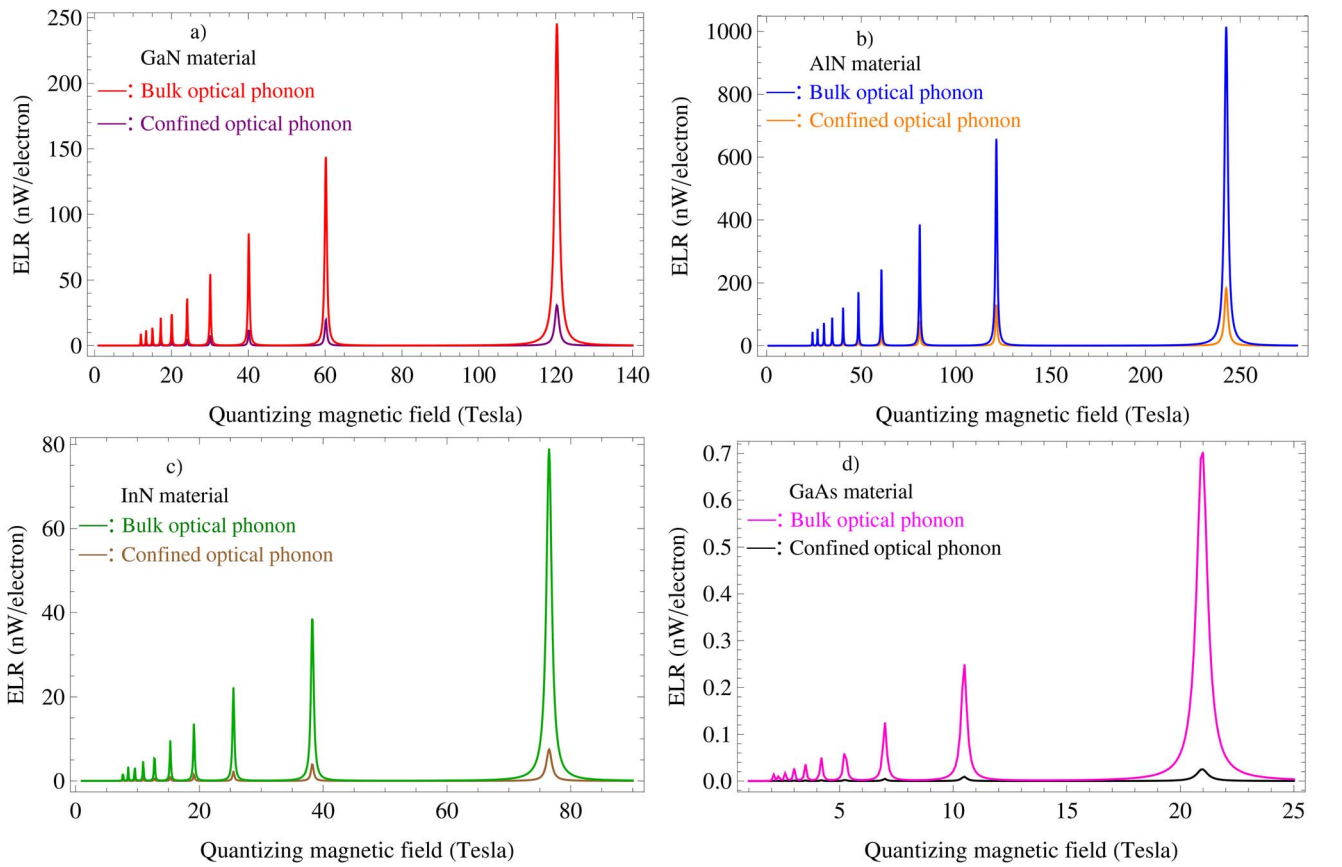

Fig. 1 Hot electron ELR compared between confined and bulk OPs and between InN, GaN, and AlN (III-nitride) and GaAs materials, as illustrated in (a–d), respectively; in a QW heterostructure *versus* the quantizing magnetic field B. In this calculation, the confined OP mode $m = 2$, width of QW $L_W = 5$ nm, lattice and electron temperatures $T_\ell = 4.2$ K and $T_e = 300$ K, and electronic concentration $n_e = 10^{16}$ m^{-2} are used. The red and purple colours for GaN refer to bulk and confined OPs, the blue and orange colours for AlN refer to bulk and confined OPs, the green and brown colours for InN refer to bulk and confined OPs, and the magenta and black colours for GaAs refer to bulk and confined OPs, respectively.

decrease, resulting in an increased scattering rate of heterostructures. This will manifest as the MPR peaks in the energy loss rate curve when graphed against the magnetic field B. Fig. 1 shows that for the InN, GaN, and AlN (III-nitride) and GaAs QW heterostructure materials, each material has 10 MPR peaks. Specifically, the MPR peaks on the B-dependent ELR graphs in the AlN, GaN, and InN (III-nitride), along with the GaAs material of the QW heterostructure corresponding to $\Delta n = 1$, occur at the quantizing magnetic field, $B = 242.61$ T, 120.32 T, and 76.49 T, along with 20.96 T, respectively for both confined and bulk OPs. Similarly, corresponding to $\Delta n = 2$ are the MPR peaks on the B-dependent ELR graphs in the materials: AlN, GaN, and InN (III-nitride), along with GaAs material at B of 121.30 T, 60.16 T, and 38.25 T, along with 10.48 T, respectively for both confined and bulk OPs, followed by $\Delta n = 3$ and so on to that at $\Delta n = 10$. The obtained findings in Fig. 1 demonstrated that the strengths of the magneto-phonon oscillation (MPO) amplitudes in InN, GaN, and AlN (III-nitride) and GaAs QW heterostructure materials rise as the magnetic field intensifies for both confined and bulk OPs. At a stronger magnetic-field, the resonant peaks have a higher MPO amplitude and are wider. The primary cause of this is because of the diminishment of the magnetic length, $\Re = \sqrt{\hbar c/(B|e|)}$, with the stronger magnetic field.[1] On the other hand, taking into account the outcomes in Fig. 1, we found that the resonant peak values of the electron ELR in the quantizing magnetic field dependence of AlN, GaN, and InN (III-nitride) and GaAs QW heterostructures corresponding to $\Delta n = 1$ obtained for confined OPs are 18.50%, 12.65%, and 9.38%; and 3.57% of those received for bulk OPs in the AlN, GaN, and InN (III-nitride); and material GaAs, respectively. Similarly, the resonant peak values of the electron ELR in the B-dependence of AlN, GaN, and InN, and GaAs QW heterostructures corresponding to $\Delta n = 2$ obtained for confined OPs are 20.05%, 13.33%, and 9.98%; and 3.46% of those received for bulk OPs in the AlN, GaN, and InN (III-nitride); and material GaAs, respectively, followed by $\Delta n = 3$ and so on. Our findings prove that the ELR in the GaAs material QW heterostructure of hot electrons is the smallest, followed by the InN and GaN material QW heterostructures, while it is the largest for the AlN material QW heterostructures in both the confinement and bulk OP interaction cases. On the other hand, the outcomes also suggest that the ELR's resonant peak values in InN, GaN, and AlN (III-nitride) and GaAs QW heterostructures of hot electrons in the confinement OP interaction case are always much smaller than

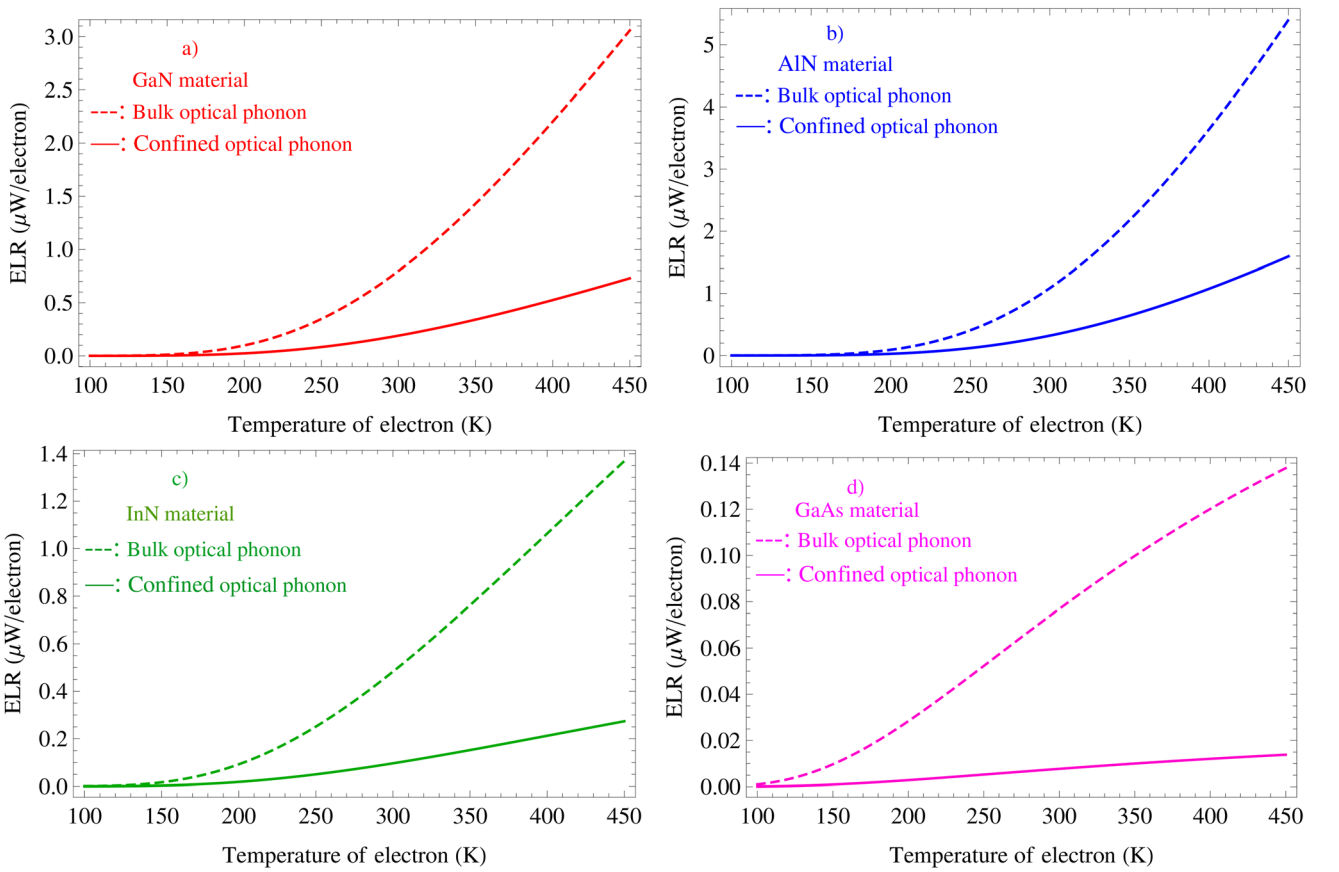

Fig. 2 Hot electron ELR compared between confined and bulk OPs and between InN, GaN, and AlN (III-nitride) and GaAs materials, as illustrated in (a–d), respectively; in a QW heterostructure *versus* the electronic temperature. In this calculation, the confined OP mode $m = 2$, width of QW $L_W = 5$ nm, temperatures of lattice $T_\ell = 4.2$ K, and electronic concentration $n_e = 10^{16}$ m^{-2} are used. Dashed red and solid red curves for GaN refer to bulk and confined OPs, dashed blue and solid blue curves for AlN refer to bulk and confined OPs, dashed green and solid green curves for InN refer to bulk and confined OPs, and dashed magenta and solid magenta curves for GaAs refer to bulk and confined OPs, respectively.

those in the bulk OP interaction case. The outcomes in this work demonstrate that the OP confinement dramatically lowers the ELR in InN, GaN, and AlN (III-nitride) and GaAs QW heterostructures of hot electrons compared to bulk OPs. The substantial difference in the resonant peak values of the electron ELR in InN, GaN, and AlN (III-nitride) and GaAs QW heterostructure materials can be ascribed to the spectrum of OP energy in each material, which satisfies $\Delta n\omega_B = \omega_{LO}{}^{q_\parallel, q_\ell}$, the resonance condition. Namely, the frequency of electronic scattering is influenced by the energy levels of each OP mode. When a certain magnetic field is introduced, the energy of a particular OP mode aligns precisely for transitions among Landau levels, leading to a peak in the response. In particular, the spectrum of confined OP energy depends on the velocity parameter β in each material, as shown in eqn (9). Hence, it is interesting to study the discrepancies in the energy relaxation rate in the InN, GaN, and AlN (III-nitride) and GaAs QW heterostructure materials of the electrons in these different materials. In addition, according to our findings, the resonant peak values of the electron ELR in the B dependence of InN, GaN, and AlN (III-nitride) and GaAs QW heterostructure materials corresponding to any Δn values obtained for confined OPs are always smaller than those received for bulk OPs. This discrepancy in the resonant peak values of the electron ELR of confined OP compared to bulk OP can be ascribed to the following four reasons: firstly, the limited number of optical confined modes that take part in the relaxation process. Secondly, the interaction between confined OPs and 2D electrons diminishes as the confined OP mode number rises because of a discrepancy between the energies of the confined OP modes and the separation of energy levels. Thirdly, the substantial reduction in the ELR of the III-nitride and GaAs QW heterostructure materials observed in the case of confined OPs compared to bulk OPs is ascribed to the change in electron-confined OP interaction strength, as well as in electron-confined OP scattering probability compared to bulk OP. Fourthly, the phonon system's dimensional reduction is manifested as a significant impairment in the electronic cooling mechanism.[57,58]

Fig. 2 is the ELR's numerical results in the III-nitride and GaAs QW heterostructure of hot electrons in the electronic temperature dependency, where two confined and bulk OP cases are illustrated. In detail, the hot electron ELR is compared between confined and bulk OPs and between InN, GaN, and AlN (III-nitride) and GaAs materials in a QW heterostructure *versus* the electronic temperature. In this calculation, the confined OP mode $m = 2$, width of QW $L_W = 5$ nm, temperatures of lattice $T_\ell = 4.2$ K, and electronic concentration $n_e = 10^{16}$ m^{-2} are used. Our findings in the figure specifically indicated that the ELRs in the III-nitride and GaAs QW heterostructure materials of hot electrons in both the confinement and bulk OP interaction cases increase with rising electronic temperature. At higher electronic temperatures, these incremental rates are faster. This can be ascribed to the fact that higher electronic temperatures allow electrons in the III-nitride and GaAs QW heterostructures to interact with a considerable amount of OP modes. In particular, in this calculation, our findings prove that the ELRs in both the III-nitride and GaAs QW heterostructure materials of hot electrons in the confinement OP interaction case varied more slowly, and they had lower values in the bulk OP interaction case. The causes of this are as follows: (i) the limited number of OP confined modes that take part in the relaxation process; (ii) the interaction between confined OPs and 2D electrons diminishes as the confined OP mode number rises because of a discrepancy between the energies of the confined

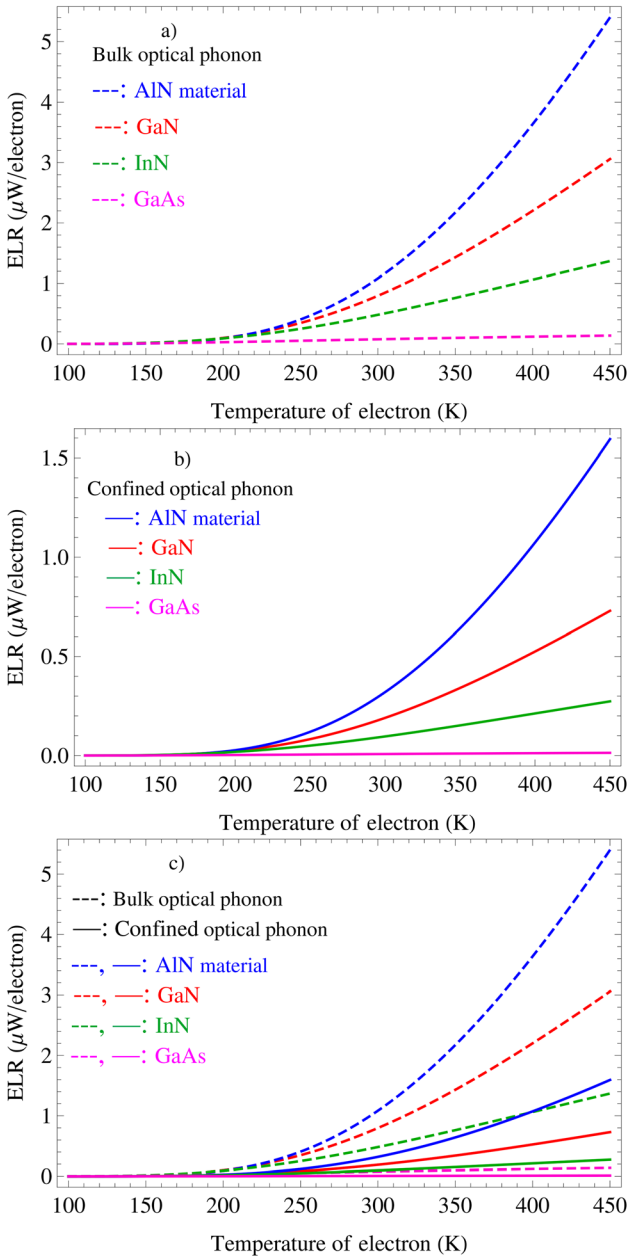

Fig. 3 The comparisons of hot electron ELR made between bulk (a) and confined (b) OPs and between InN, GaN, and AlN (III-nitride) and GaAs materials in a QW heterostructure *versus* the electronic temperature. The comparison of bulk with confined phonons for all four materials is presented in (c). In this calculation, the confined OP mode $m = 2$, width of QW $L_W = 5$ nm, temperature of lattice $T_\ell = 4.2$ K, and electronic concentration $n_e = 10^{16}$ m^{-2} are used. The dashed and solid lines refer to bulk and confined OPs; the blue, red, green, and magenta colours refer to AlN, GaN, InN, and GaAs, respectively.

OP modes and the separation of energy levels; (iii) the substantial reduction in the InN, GaN, AlN, and GaAs QW heterostructure materials observed in the case of confined OPs compared to bulk OPs is ascribed to the modification in the spectrum of confined OP-energy involved in the confined electron-confined OP interaction; (iv) the phonon system's dimensional reduction is manifested as a significant impairment in the electronic cooling mechanism. On the other hand, the figure additionally shows that there is a substantial difference in the resonant peak values of the electron ELR of InN, GaN, and AlN, and GaAs materials in the electronic temperature dependency. This feature will be more explicitly shown and discussed specifically in Fig. 3 for both cases of the confined and bulk OPs.

Two confined and bulk OP cases are shown in Fig. 3, which shows the numerical results of the ELR in the III-nitride and GaAs QW heterostructures of hot electrons in the electronic temperature dependency. In more detail, we provided the comparative results between the four (InN, GaN, AlN, and GaAs) materials for bulk OPs in Fig. 3(a), for confined OPs in Fig. 3(b), and for both comparison of confined and bulk OPs in Fig. 3(c). In this calculation, the confined OP mode $m = 2$, width of QW $L_W = 5$ nm, temperature of lattice $T_\ell = 4.2$ K, and electronic concentration $n_e = 10^{16}$ m^{-2} are used. Our results in the figure explicitly showed that the ELRs in the InN, GaN, and AlN (III-nitride) and GaAs QW heterostructure materials of hot electrons in both the confined (Fig. 3(b)) and bulk (Fig. 3(a)) OP interaction cases increase with rising electronic temperature. For both the confined and bulk OP interaction cases, at higher electronic temperatures, these incremental rates are faster in all the InN, GaN, AlN, and GaAs QW heterostructure materials. In addition, our findings obtained also indicate that the electronic temperature dependency of the ELR in the III-nitride QW heterostructure is stronger than that in the GaAs material QW heterostructure for both the confinement and bulk OP interaction cases. Specifically, the ELRs in the InN, GaN, and AlN (III-nitride) QW heterostructures of hot electrons varied more rapidly, and they had higher values compared to the GaAs QW heterostructure for both the confinement (shown in Fig. 3(b)) and bulk (shown in Fig. 3(a)) OP interaction cases. On the other hand, in a comparison between the InN, GaN, and AlN (III-nitride) QW heterostructures, according to the obtained outcome in the figure, the ELR in the AlN material heterostructure of hot electrons varied the fastest and had the highest value; however, that for the InN material heterostructure varied the slowest and had the lowest value, *i.e.*, the ELR's electronic

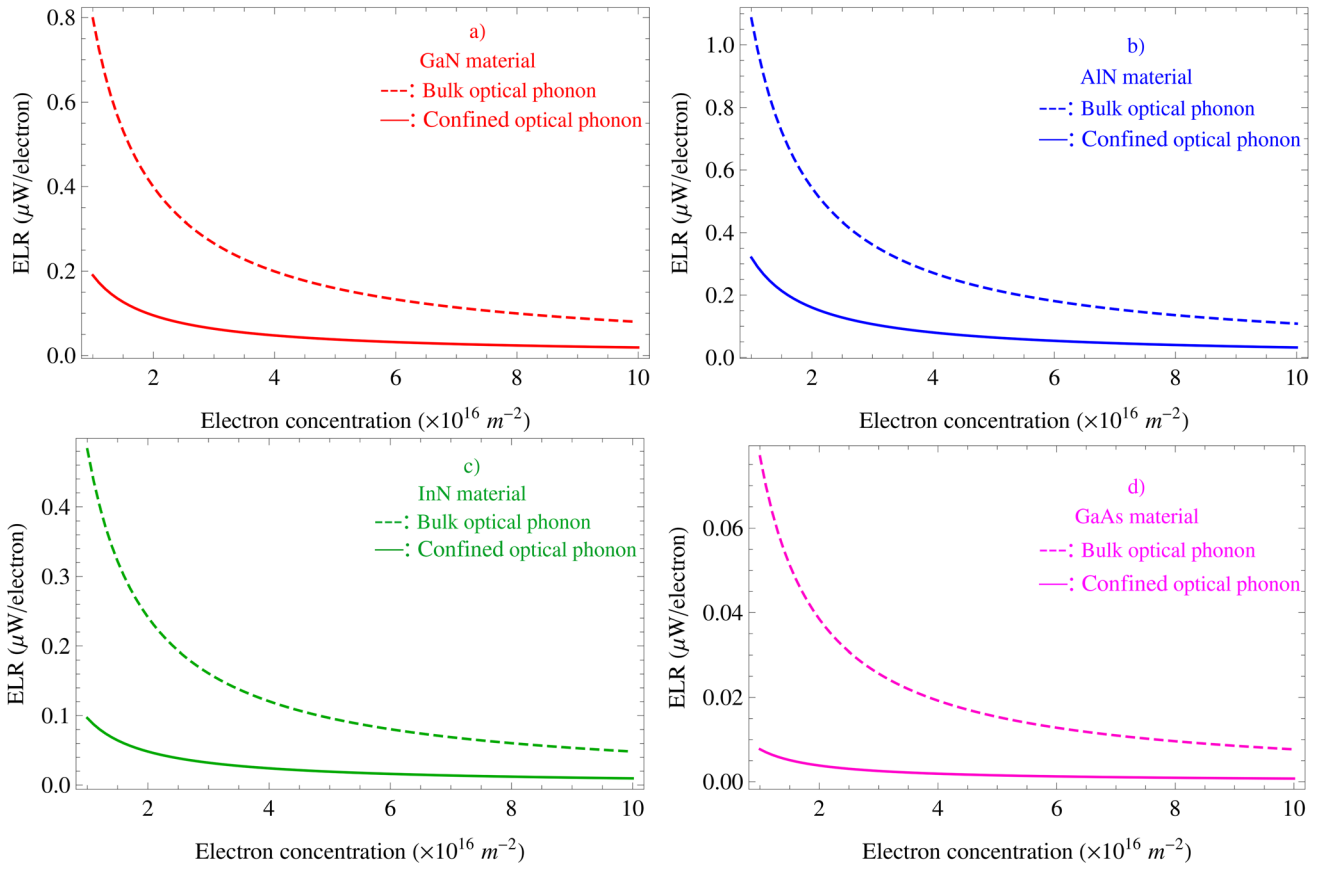

Fig. 4 Hot electron ELR compared between confined and bulk OPs and between InN, GaN, and AlN (III-nitride) and GaAs materials, as illustrated in (a–d), respectively; in a QW heterostructure *versus* the electronic concentration. In this calculation, the confined OP mode $m = 2$, width of QW $L_W = 5$ nm, and lattice and electron temperatures $T_\ell = 4.2$ K and $T_e = 300$ K are used. Dashed red and solid red curves for GaN refer to bulk and confined OPs, dashed blue and solid blue curves for AlN refer to bulk and confined OPs, dashed green and solid green curves for InN refer to bulk and confined OPs, and dashed magenta and solid magenta curves for GaAs refer to bulk and confined OPs, respectively.

temperature dependency of hot electrons in the AlN material heterostructure is the strongest; by contrast, that for the InN material heterostructure is the weakest for both the confinement and bulk OP interaction cases. Hence, it is interesting to study the discrepancies in the energy relaxation rate in the InN, GaN, and AlN, and GaAs QW heterostructure materials of the electrons in these different materials. Insights gained from these discoveries could significantly contribute to the advancement of optoelectronic device fabrication. Furthermore, to elucidate the influence of confined OPs on the ELR in the III-nitride and GaAs QW heterostructures compared to bulk OPs, we provided the comparative findings in Fig. 3(c). It was shown by the data that the OP confinement significantly reduces the ELR in the InN, GaN, and AlN (III-nitride) and GaAs QW heterostructure materials of hot electrons, *i.e.*, the ELRs in the III-nitride and GaAs QW heterostructure materials of hot electrons in the confinement OP interaction case varied more slowly and had lower values than the bulk OP interaction case. In particular, we were able to see that among these four QW heterostructure materials (InN, GaN, AlN, and GaAs), the ELR in the GaAs material QW heterostructure of hot electrons is the smallest; in the AlN material QW heterostructure, it is the largest. In addition to the study of the electronic temperature dependency of the ELR, the quantum-well width and electronic concentration dependencies are also examined in detail, and their results are shown in the figures below.

The numerical computation outcomes of the ELR in the III-nitride and GaAs QW heterostructure of hot electrons in the electronic concentration dependency are shown in Fig. 4, which illustrates two confined and bulk OP cases. Here, the hot electron ELR is compared between confined and bulk OPs and between InN, GaN, and AlN (III-nitride) and GaAs materials in a QW heterostructure *versus* the electronic concentration. In this calculation, the confined OP mode $m = 2$, width of QW $L_W = 5$ nm, and lattice and electron temperatures $T_\ell = 4.2$ K and $T_e = 300$ K are used. As the figure illustrates, with rising surface concentrations, the ELRs in InN, GaN, AlN, and GaAs material QW heterostructures of hot electrons in the confinement and bulk OP interaction cases reduce visibly. In particular, in this calculation, our findings also prove that the ELRs in both the InN, GaN, and AlN (III-nitride) and GaAs QW heterostructure materials of hot electrons in the confined OP interaction case varied more slowly, and they had lower values in the bulk OP interaction case. This feature is due to the limited number of optical confined modes that take part in the relaxation process. Moreover, the interaction between confined OPs and 2D electrons diminishes as the confined OP mode number rises because of a discrepancy between the energies of the confined OP modes and the separation of energy levels. Besides, the substantial reduction in the InN, GaN, AlN, and GaAs QW heterostructure materials observed in the case of confined OPs compared to bulk OPs is ascribed to the modification in the spectrum of confined OP-energy involved in the confined electron-confined OP interaction. In addition, the phonon system's dimensional reduction is manifested as a significant impairment in the electronic cooling mechanism. Concurrently, at higher surface concentrations, the differences in the value and the variation of the ELRs between the confinement and bulk OP interaction cases are small and insignificant in all InN, GaN, AlN, and GaAs material QW heterostructures. However, the dependency of the ELR in the InN, GaN, AlN, and GaAs QW heterostructures on the surface concentration is very different in both the confinement and bulk OP interaction cases, as explicitly shown and discussed specifically in Fig. 5 below.

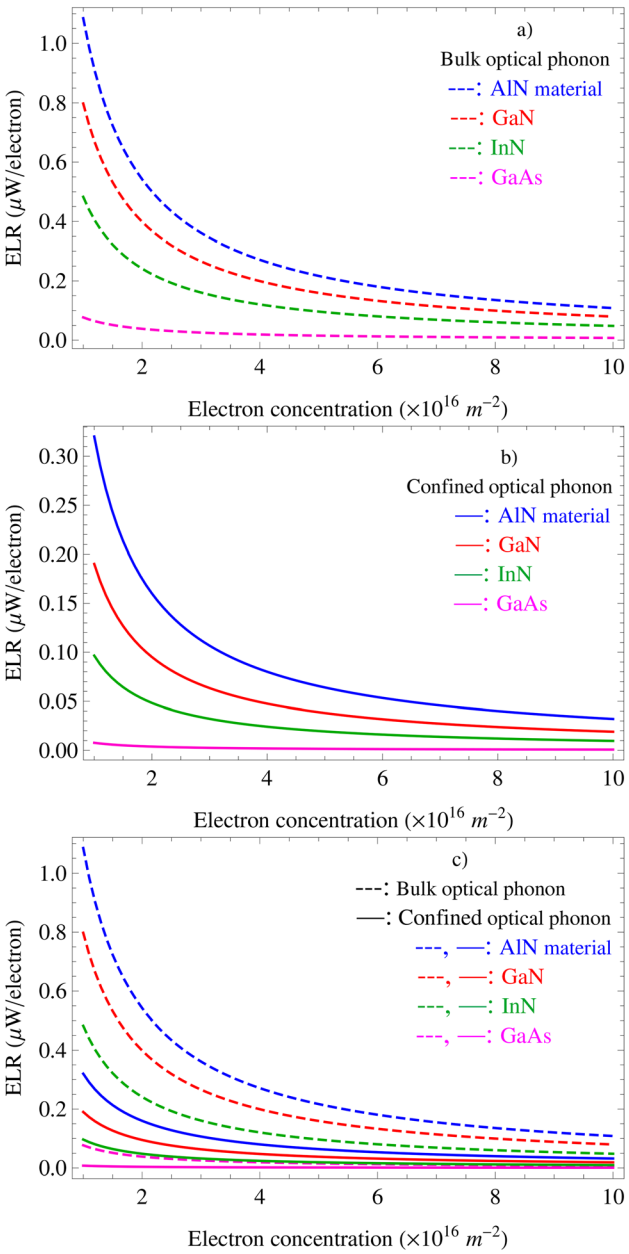

Fig. 5 Comparison of hot electron ELR between confined and bulk OPs and between InN, GaN, and AlN (III-nitride) and GaAs materials, as illustrated in (a–c), respectively; in a QW heterostructure *versus* the electronic concentration. In this calculation, the confined OP mode $m = 2$, width of QW $L_W = 5$ nm, and lattice and electron temperatures $T_\ell = 4.2$ K and $T_e = 300$ K are used. The dashed and solid lines refer to bulk and confined OPs; the blue, red, green, and magenta colours refer to AlN, GaN, InN, and GaAs, respectively.

Fig. 5 is the detailed comparative result of hot electron ELR between confined and bulk OPs and between InN, GaN, and AlN (III-nitride) and GaAs materials in a QW heterostructure *versus* the electronic concentration. In this calculation, the confined OP mode $m = 2$, width of QW $L_W = 5$ nm, and lattice and electron temperatures $T_\ell = 4.2$ K and $T_e = 300$ K are used. Here, the comparative results between the four (AlN, GaN, InN, and GaAs) materials for bulk OPs are shown in Fig. 5(a), for confined OPs in Fig. 5(b), and for both confined and bulk OPs in Fig. 5(c). Our findings in the figure prove that the ELRs in the InN, GaN, and AlN (III-nitride) and GaAs QW heterostructure materials of hot electrons in both the confined (Fig. 5(b)) and bulk (Fig. 5(a)) OP interaction cases diminished with rising surface concentrations. In all the AlN, GaN, InN, and GaAs QW heterostructure materials, these diminishable rates are faster at lower surface concentrations for both the confinement and bulk OP interaction cases. Furthermore, for both the confinement and bulk OP interaction cases, our results also show that the surface concentration dependency of the ELR in the GaAs QW heterostructure is weaker than that in the III-nitride QW heterostructures. Namely, the ELRs in the GaAs QW heterostructure of hot electrons varied more slowly, and they had lower values compared to the InN, GaN, and AlN (III-nitride) QW heterostructures for both the confinement (shown in Fig. 5(b)) and bulk (shown in Fig. 5(a)) OP interaction cases. In the present study, it is fascinating to study the discrepancies in the energy relaxation rate in the InN, GaN, and AlN, and GaAs QW heterostructure materials of the electron in these various materials. Specifically, in a comparison between the InN, GaN, and AlN (III-nitride) QW heterostructures, according to the obtained outcome in the figure, the ELR in the AlN material heterostructure of hot electrons varied the fastest and had the highest value; however, that for the InN material heterostructure varied the slowest and had the lowest value, *i.e.*, the ELR's surface concentration dependency of hot electrons in the AlN material heterostructure is the strongest; by contrast, that for the InN material heterostructure is the weakest for both the confinement and bulk OP interaction cases. Therefore, the knowledge gathered from these findings may greatly aid the development of optoelectronic devices. Additionally, we presented the comparative results in Fig. 5(c) to clarify the impact of confined OPs on the ELR in the III-nitride and GaAs QW heterostructures compared to bulk OPs. According to the figure, our findings prove that the ELR in the GaAs material QW

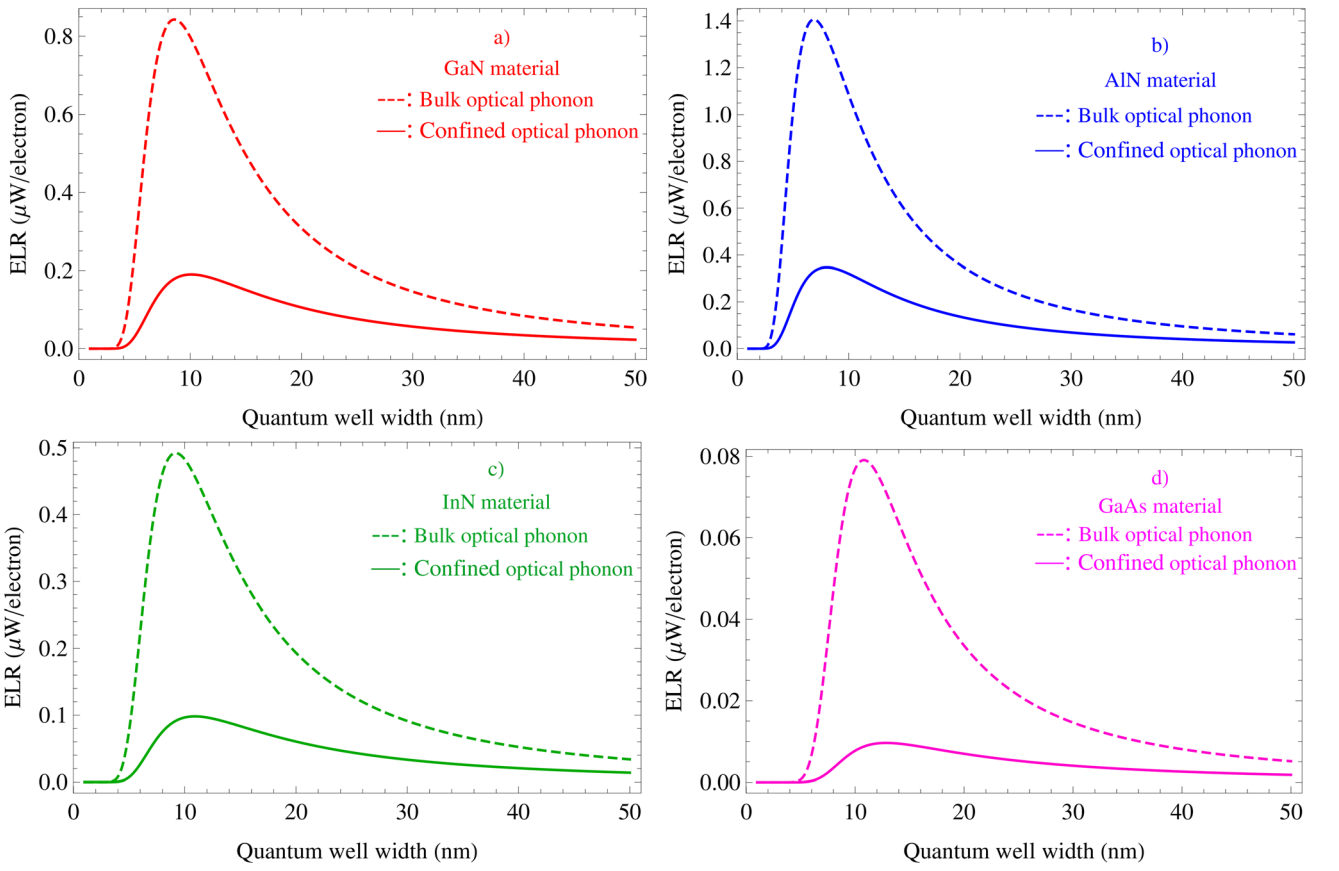

Fig. 6 Hot electron ELR compared between confined and bulk OPs and between InN, GaN, and AlN (III-nitride) and GaAs materials, as illustrated in (a–d), respectively; in a QW heterostructure *versus* the width of QW. In this calculation, the confined OP mode $m = 2$, lattice and electron temperatures $T_\ell = 4.2$ K and $T_e = 300$ K, and electronic concentration $n_e = 10^{16}$ m^{-2} are used. Dashed red and solid red curves for GaN refer to bulk and confined OPs, dashed blue and solid blue curves for AlN refer to bulk and confined OPs, dashed green and solid green curves for InN refer to bulk and confined OPs, and dashed magenta and solid magenta curves for GaAs refer to bulk and confined OPs, respectively.

heterostructure of hot electrons is the smallest, followed by that in the InN, and GaN material QW heterostructures, while it is the largest for the AlN material QW heterostructures in both the confinement and bulk OP interaction cases. The data proved that the OP confinement dramatically lowers the ELR in both the InN, GaN, and AlN (III-nitride) and GaAs QW heterostructure materials of hot electrons, *i.e.*, comparing the confinement OP interaction case to the bulk OP interaction case, the ELRs in the III-nitride and GaAs QW heterostructure materials of hot electrons varied more slowly and had lower values. Therefore, our findings proved that the OP confinement greatly affects the ELRs in the InN, GaN, and AlN (III-nitride) and GaAs QW heterostructure materials of hot electrons. Specifically, it significantly reduces the ELR in InN, GaN, and AlN (III-nitride) and GaAs QW heterostructure materials of hot electrons compared to bulk OPs. More importantly, the impact of the quantum-well width on the ELRs in the III-nitride and GaAs QW heterostructure materials of hot electrons in this study, taking into account the OP confinement, is also shown in Fig. 6 and 7 below.

The numerical results of the ELR in the III-nitride and GaAs QW heterostructure of hot electrons in the quantum-well width dependency are provided in Fig. 6, which shows two confined and bulk OP cases. Specifically, the hot electron ELR is compared between confined and bulk OPs and between InN, GaN, and AlN (III-nitride) and GaAs materials in a QW heterostructure *versus* the width of QW. In this calculation, the confined OP mode $m = 2$, lattice and electron temperatures $T_\ell = 4.2$ K and $T_e = 300$ K, and electronic concentration $n_e = 10^{16}$ m^{-2} are used. The graph implies that the ELR in the InN, GaN, and AlN (III-nitride) and GaAs QW heterostructures of hot electrons in both the confinement and bulk OP interaction cases is a function of the QW heterostructure width. Additionally, our data suggest that the ELR in the InN, GaN, and AlN (III-nitride) and GaAs QW heterostructures of hot electrons is highly dependent on these heterostructure material properties; nevertheless, this dependence is negligible when the quantum-well heterostructure width is larger than 40 nm. This is shown explicitly in the figure by the different values of the ELR in different QW heterostructure materials, such as InN, GaN, AlN, and GaAs. At the same time, the graph also implies that when the quantum-well heterostructure width is larger than 40 nm, the influence of OP confinement on the ELR in the III-nitride and GaAs QW heterostructures of hot electrons is negligible and can be disregarded. Conversely, however, when the quantum-well heterostructure width is sufficiently small (smaller than 20 nm), the features of the ELR, including the variation and value of the electron ELR, are strongly dependent on material properties of the InN, GaN, and AlN (III-nitride) and GaAs QW heterostructures; concurrently, the OP confinement greatly affects the ELR in the III-nitride and GaAs QW heterostructures of hot electrons, *i.e.*, it significantly reduces the ELR in these QW heterostructure materials of hot electrons compared to bulk OPs. Hence, when the size of the InN, GaN, and AlN (III-nitride) and GaAs QW heterostructure materials is decreased, their chemical and physical characteristics drastically change, leading to properties because of the effect of their quantum size.

Fig. 7 displays two confined and bulk OP cases of the ELR numerical results in the III-nitride and GaAs QW heterostructure of hot electrons in the quantum-well width dependency. In particular, the comparison of hot electron ELRs between confined and bulk OPs and between InN, GaN, and AlN (III-nitride) and GaAs materials in a QW heterostructure *versus*

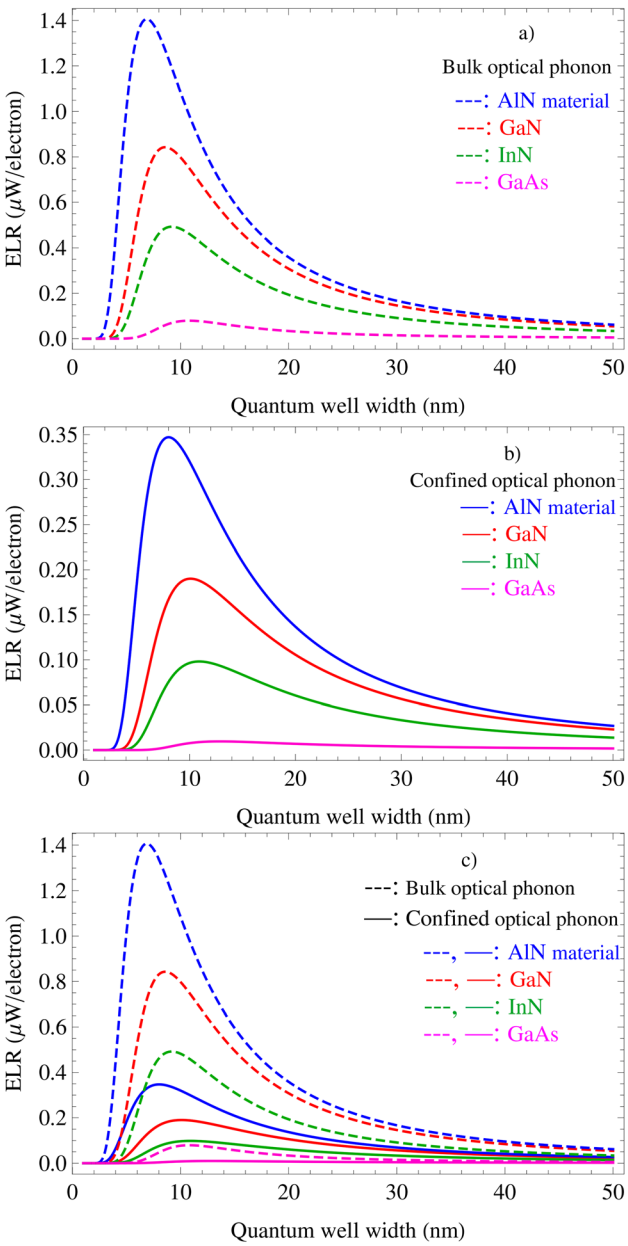

Fig. 7 Comparison of hot electron ELR between confined and bulk OPs and between InN, GaN, and AlN (III-nitride) and GaAs materials, as illustrated in (a–c), respectively; in a QW heterostructure *versus* the width of QW. In this calculation, the confined OP mode $m = 2$, lattice and electron temperatures $T_\ell = 4.2$ K and $T_e = 300$ K, and electronic concentration $n_e = 10^{16}$ m^{-2} are used. The dashed and solid lines refer to bulk and confined OPs; the blue, red, green, and magenta colours refer to AlN, GaN, InN, and GaAs, respectively.

the width of QW is made in detail. In this calculation, the confined OP mode $m = 2$, lattice and electron temperatures $T_\ell = 4.2$ K and $T_e = 300$ K, and electronic concentration $n_e = 10^{16}$ m^{-2} are used. In greater detail, the comparative results between the four (AlN, GaN, InN, and GaAs) materials for bulk OPs are shown in Fig. 7(a), for confined OPs in Fig. 7(b), and for both confined and bulk OPs in Fig. 7(c). We can make the following deductions after examining the outcome in Fig. 7: firstly, the ELR in the InN, GaN, AlN, and GaAs material QW heterostructures of hot electrons in both the confinement and bulk OP interaction cases is a function of the QW heterostructure width. This characteristic undeniably proves that the ELR in the InN, GaN, and AlN (III-nitride) and GaAs QW heterostructures of hot electrons can be controlled by changing the QW heterostructure width. Secondly, the position and value of the electron ELR's resonant peak are different for the different QW heterostructure materials InN, GaN, AlN, and GaAs. This feature implies that the material properties greatly impact the ELR in the InN, GaN, and AlN (III-nitride) and GaAs QW heterostructures of hot electrons in the quantum-well heterostructure width dependency. Simultaneously, the influence of the material properties of the InN, GaN, and AlN (III-nitride) and GaAs QW heterostructure materials on the quantum-well heterostructure width dependency of the ELR becomes more pronounced when the quantum-well heterostructure width is small enough, *i.e.*, $L_W < 20$ nm. Thirdly, among the four (InN, GaN, AlN, and GaAs) QW heterostructure materials, the quantum-well heterostructure width dependency of the ELR in the GaAs material QW heterostructure of hot electrons is the weakest, followed by the InN and GaN material QW heterostructures, whereas it is the strongest for the AlN material QW heterostructures in both the confinement (shown in Fig. 7(b)) and bulk (shown in Fig. 7(a)) OP interaction cases. Fourthly, upon comparison between group InN, GaN, and AlN (III-nitride) materials, the obtained graph showed that the ELR in the AlN material heterostructure of hot electrons varied the fastest and had the highest value; however, that for the InN material heterostructure varied the slowest and had the lowest value, *i.e.*, the QW heterostructure width dependency of the ELR in the AlN material heterostructure of hot electrons is the strongest; by contrast, that for the InN material heterostructure is the weakest for both the confinement and bulk OP interaction cases. Fifthly, the data in Fig. 7(c) proved that the OP confinement dramatically lowers the ELR in both the InN, GaN, and AlN (III-nitride) and GaAs QW heterostructure materials of hot electrons, *i.e.*, comparing the confinement OP interaction case to the bulk OP interaction case, the ELRs in the III-nitride and GaAs QW heterostructure materials of hot electrons varied more

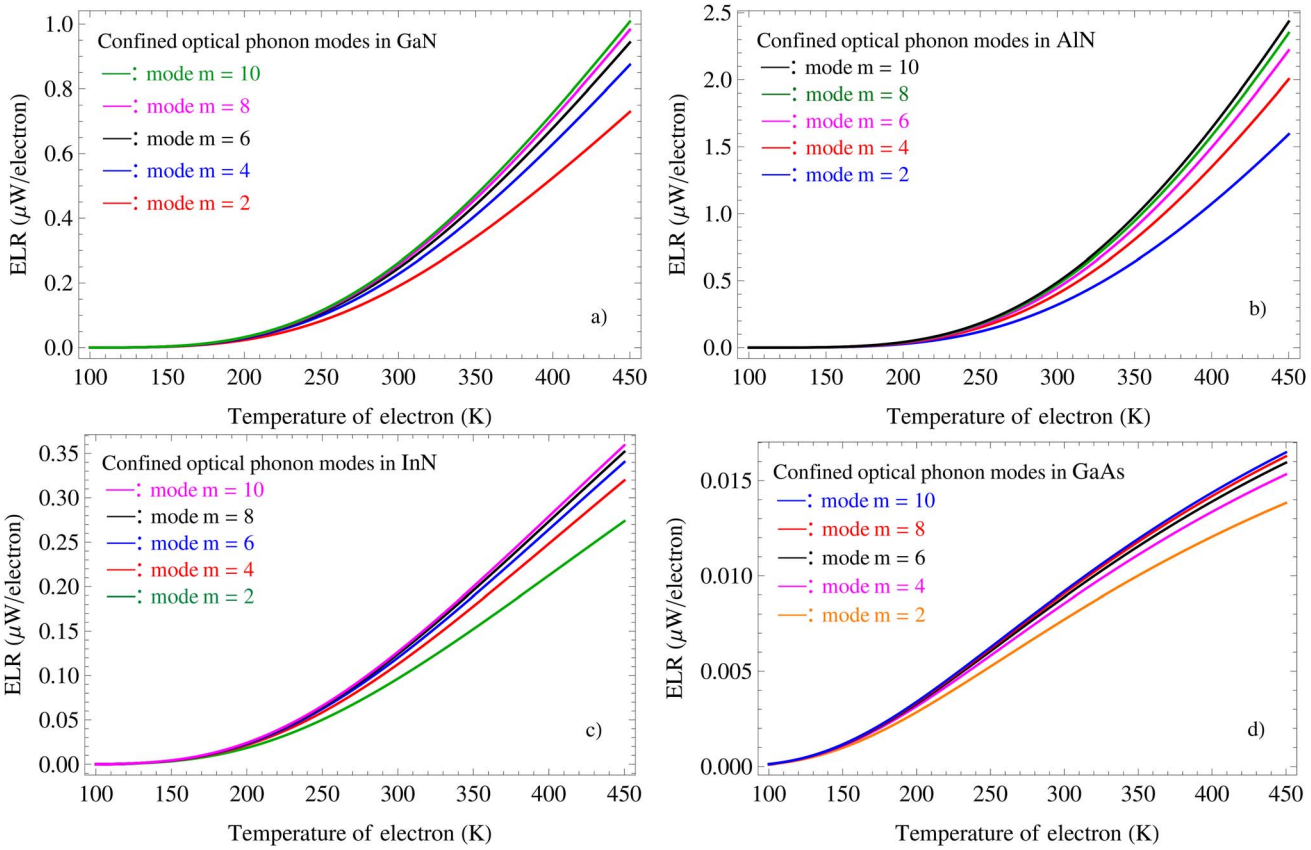

Fig. 8 The different contributions of confined OP modes to hot electron ELR compared between InN, GaN, and AlN (III-nitride) and GaAs materials in a QW heterostructure *versus* the electronic temperature. In this calculation, width of QW $L_W = 5$ nm, temperature of lattice $T_\ell = 4.2$ K, and electronic concentration $n_e = 10^{16}$ m^{-2} are used. Here, the confined OP modes $m = 2$, 4, 6, 8, and 10 are compared to each material in detail, and (a–d) refer to GaN, AlN, and InN materials, and GaAs, respectively.

slowly and had lower values. Sixthly, the MPR-peak position of the ELR in the InN, GaN, and AlN (III-nitride) and GaAs QW heterostructure materials of hot electrons in the quantum well heterostructure width dependency displaced to a smaller quantum-well width. Here, the strength of the peak shift in the AlN material QW heterostructure is the greatest, followed by that in the GaN and InN material QW heterostructures, whereas that in the GaAs material QW heterostructure is the weakest for both the confinement and bulk OP interaction cases. This has to do with the OP energy of the corresponding materials, where the OP energy of the AlN is the largest, followed by that of the GaN and InN, whereas that of the GaAs is the smallest. Thus, the OP confinement greatly affects the ELRs in the InN, GaN, and AlN (III-nitride) and GaAs QW heterostructure materials of hot electrons. At the same time, when the quantum-well heterostructure width is small enough, the difference between the confinement and bulk OP interactions is considerable in the research of the ELR in the InN, GaN, and AlN (III-nitride) and GaAs QW heterostructures of hot electrons in these quasi-2D systems. Therefore, when studying the ELR in semiconductor heterostructures of hot electrons, OP confinement must be considered. Insights gained from these discoveries could significantly contribute to the advancement of optoelectronic device fabrication, such as waveguides, laser technology, light-emitting nanodevices, *etc.* Significant advancements in the semiconductor industry will undoubtedly result from further development of this nanotechnology.

In Fig. 8, we show the different contributions of confined OP modes to hot electron ELR compared between InN, GaN, and AlN (III-nitride) and GaAs materials in a QW heterostructure *versus* the electronic temperature. In this calculation, width of QW $L_W = 5$ nm, temperature of lattice $T_\ell = 4.2$ K, and electronic concentration $n_e = 10^{16}$ m^{-2} are used. Here, the confined OP modes $m = 2$, 4, 6, 8, and 10 are compared to each material in detail, and Fig. 8(a)–(d) refer to GaN, AlN, and InN materials, and GaAs material, respectively. In this figure, we have obtained the data for the variation of the ELR in the InN, GaN, and AlN (III-nitride) and GaAs QW heterostructures of hot electrons with their temperature at the first five confined OP modes, $m = 2$, 4, 6, 8, and 10. Following the outcome analysis in Fig. 8(b), we can make the following deductions: (i) the ELRs in the InN, GaN, and AlN (III-nitride) and GaAs QW heterostructures of hot electrons are functions of their temperature at the different confined OP modes; (ii) the ELRs in the InN, GaN, and AlN (III-nitride) and GaAs QW heterostructures of hot electrons increase with rising electronic temperature for all the confined OP modes; (iii) the contribution of the various confined OP modes, $m = 2$, 4, 6, 8, and 10, to the ELRs in the InN, GaN, and AlN (III-

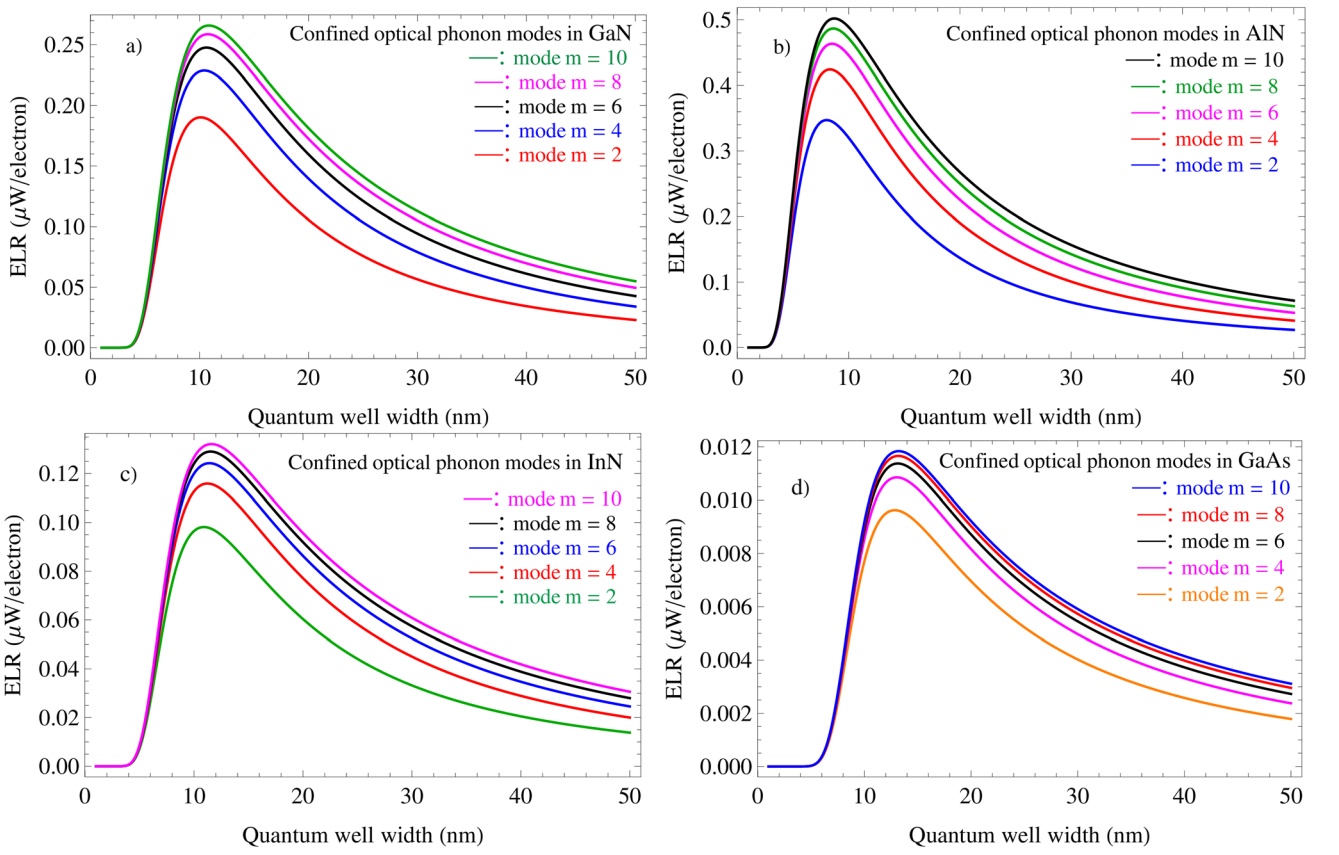

Fig. 9 The different contributions of confined OP modes to hot electron ELR compared between InN, GaN, and AlN (III-nitride) and GaAs materials in a QW heterostructure *versus* the width of QW. In this calculation, lattice and electron temperatures $T_\ell = 4.2$ K and $T_e = 300$ K, and electronic concentration $n_e = 10^{16}$ m^{-2} are used. Here, the confined OP modes $m = 2$, 4, 6, 8, and 10 are compared to each material in detail, and (a–d) refer to GaN, AlN, and InN materials, and GaAs, respectively.

nitride) and GaAs QW heterostructures of hot electrons are different. This difference in contribution can be determined more clearly at higher electronic temperatures; (iv) among the first five confined OP modes, $m = 2$, 4, 6, 8, and 10, the ELR in the InN, GaN, and AlN (III-nitride) and GaAs QW heterostructures of hot electrons in the electronic temperature dependency for the confined OP mode, $m = 10$, increased the fastest and had the highest value, followed by that of the confined OP mode, $m = 8$, $m = 6$, and $m = 4$, whereas that for the confined OP mode, $m = 2$, increased the slowest and had the lowest value. Therefore, the ELR in the InN, GaN, and AlN (III-nitride) and GaAs QW heterostructures of hot electrons is the smallest for the lowest confined OP mode. In particular, the contribution of the confined OP modes, 6, 8, 10, *etc.* (from the third mode onwards) to the ELR in the III-nitride and GaAs QW heterostructures of hot electrons differs only slightly and is negligible.

Finally, Fig. 9 is the specific result of the different contributions of confined OP modes to hot electron ELR compared between InN, GaN, and AlN (III-nitride) and GaAs materials in a QW heterostructure *versus* the width of QW. In this calculation, lattice and electron temperatures $T_\ell = 4.2$ K and $T_e = 300$ K, and electronic concentration $n_e = 10^{16}$ m^{-2} are used. Here, the confined OP modes $m = 2$, 4, 6, 8, and 10 are compared to each material in detail, and Fig. 9(a)–(d) refer to GaN, AlN, InN, and GaAs, respectively. To obtain additional proof of the various contributions from individual confined OP modes, especially the two lowest confined OP modes, to the ELR in the III-nitride and GaAs QW heterostructures of hot electrons, we have additionally examined the quantum well heterostructure width dependency of the ELR in the InN, GaN, AlN, and GaAs materials at individual confined OP modes and obtained the following results: the ELRs in the InN, GaN, AlN, and GaAs QW heterostructures of hot electrons are functions of the quantum well heterostructure width at individual confined OP modes. Similarly to information found in Fig. 8, among confined OP modes, $m = 2$, 4, 6, 8, and 10, the ELR in the InN, GaN, AlN, and GaAs QW heterostructures of hot electrons in the quantum well heterostructure width dependency for the confined OP mode, $m = 10$, varied the fastest and had the highest value, followed by that for the confined OP mode, $m = 8$, $m = 6$, and $m = 4$, whereas that for the confined OP mode, $m = 2$, varied the slowest and had the lowest value. Namely, in this case, the ELR in the III-nitride and GaAs QW heterostructures of hot electrons is still the smallest for the lowest confined OP mode. Note that the contributions from the confined OP modes, including the lowest confined OP mode, to the ELR in the III-nitride and GaAs QW heterostructures of hot electrons differs only slightly and is negligible at large widths of the quantum wells. On the other hand, the contribution from individual confined OP modes to the ELR in the III-nitride and GaAs QW heterostructures of hot electrons is sensitive to the small enough QW heterostructure width. Thus, the QW heterostructure width can be utilized as a useful tool to control the ELR in the InN, GaN, and AlN (III-nitride) and GaAs QW heterostructures of hot electrons when electrons interacting with confined OPs become the dominant scattering mechanism.

5 Conclusions

The energy loss rate in the III-nitride (InN, AlN, and GaN) and GaAs QW heterostructures of hot electrons because of confined OP scattering has been studied with the help of the electronic temperature model, the framework of confinement of OPs proposed by Huang and Zhu, and under the impact of a quantizing magnetic field. Numerical calculations of the variations of the hot-electron ELR with the quantizing magnetic field, two-dimensional electronic concentration, temperature of the two-dimensional electrons, and QW heterostructure width have been carefully compared between the InN, GaN, and AlN, and GaAs QW heterostructures for all three cases of OPs, including bulk, confinement, and both bulk and confinement. More importantly, the different contributions of individual confined OP modes to the hot-electron ELR in the InN, GaN, and AlN, and GaAs nanoscale structures have also been presented for comparison. We finally would like to offer the following results of the optoelectronic properties of the InN, GaN, and AlN (III-nitride) and GaAs QW heterostructures in this study: (i) the resonant peak values of the ELR in the quantizing magnetic field dependence of InN, GaN, and AlN (III-nitride) and GaAs QW heterostructures in the confinement OP interaction case are always much smaller than those in the bulk OP interaction case. The ELR in the GaAs material QW heterostructure of hot electrons is the smallest, followed by the InN and GaN material QW heterostructures, whereas it is the largest for the AlN material QW heterostructures in both the confinement and bulk OP interaction cases. Hence, the OP confinement dramatically lowers the ELR in InN, GaN, and AlN (III-nitride) and GaAs QW heterostructures of hot electrons compared to bulk OPs. (ii) The ELRs in the InN, GaN, and AlN (III-nitride) and GaAs QW heterostructures of hot electrons in both the confinement and bulk OP interaction cases increase with rising electronic temperature and reduce with rising surface concentrations and quantum well heterostructure width. The ELRs in the InN, GaN, and AlN (III-nitride) and GaAs QW heterostructures of hot electrons in both the confinement and bulk OP interaction cases are functions of the surface concentrations, quantum-well heterostructure width, and electronic temperature. At higher electronic temperatures, these incremental rates are faster, whereas at lower surface concentrations as well as lower quantum well heterostructure widths, these decrement rates are faster. At higher surface concentrations, the differences in the value and the variation of the ELRs between the confinement and bulk OP interaction cases are small and insignificant in all InN, GaN, AlN, and GaAs material QW heterostructures. (iii) The ELR in the InN, GaN, and AlN (III-nitride) and GaAs QW heterostructures of hot electrons is highly dependent on these heterostructure material properties; nevertheless, this dependence is negligible when the quantum-well heterostructure width is larger than 40 nm. Simultaneously, when the quantum-well heterostructure width is larger than 40 nm, the influence of OP confinement on the ELR in the III-nitride and GaAs QW heterostructures of hot electrons is negligible and can be disregarded. Conversely, however, when the quantum-well

heterostructure width is sufficiently small (smaller than 20 nm), the features of the ELR, including the value and variation of the electron ELR, are strongly dependent on the material properties of the InN, GaN, and AlN (III-nitride) and GaAs QW heterostructures; concurrently, the OP confinement greatly affects the ELR in the III-nitride and GaAs QW heterostructures of hot electrons, *i.e.*, it significantly reduces the ELR in these QW heterostructure materials of hot electrons compared to bulk OPs. The OP system's dimensional reduction is manifested as a significant impairment in the electronic cooling mechanism. Hence, when the size of the InN, GaN, and AlN (III-nitride) and GaAs QW heterostructure materials is decreased, their chemical and physical characteristics drastically change, leading to properties because of the effect of their quantum size. (iv) In a comparison between III-nitride materials (InN, AlN, and GaN), the hot electron ELR in the InN is the smallest; nevertheless, when comparing III-nitride materials (InN, AlN, and GaN) to the GaAs material, the hot electron ELR in the GaAs is the smallest. Hence, it is fascinating to study the discrepancies in the energy relaxation rate in the InN, GaN, AlN, and GaAs QW heterostructure materials of the electrons in these different materials. Insights gained from these discoveries could significantly contribute to the advancement of optoelectronic device fabrication. (v) Among individual confined OP modes, $m = 2$, 4, 6, 8, and 10, the hot electron ELR in all the InN, GaN, and AlN (III-nitride) and GaAs QW heterostructures varied the fastest and had the highest value for the $m = 10$ mode, followed for the $m = 8$, $m = 6$, and $m = 4$ modes, whereas that for the $m = 2$ mode varied the slowest and had the lowest value. Therefore, the ELR in the InN, GaN, and AlN (III-nitride) and GaAs QW heterostructures of hot electrons is the smallest for the lowest confined OP mode. Therefore, the knowledge gathered from these findings may greatly aid the optoelectronic device development.

Conflicts of interest

There are no conflicts to declare.

Data availability

The authors confirm that the data supporting the findings of this study are available within the article.

References

1 T. N. Bich, S. S. Kubakaddi, L. Dinh, N. N. Hieu and H. V. Phuc, *Phys. Rev. B*, 2021, **103**, 235417.
2 S. S. Kubakaddi and H. V. Phuc, *Semicond. Sci. Technol.*, 2020, **36**, 025005.
3 S. Das Sarma, J. K. Jain and R. Jalabert, *Phys. Rev. B: Condens. Matter Mater. Phys.*, 1990, **41**, 3561–3571.
4 R. Fletcher, J. J. Harris, C. T. Foxon and R. Stoner, *Phys. Rev. B: Condens. Matter Mater. Phys.*, 1992, **45**, 6659–6669.
5 J. S. Bhat, S. B. Kapatkar, S. S. Kubakaddi and B. G. Mulimani, *Phys. Status Solidi B*, 1998, **209**, 37–47.
6 A. L. Vartanian, A. L. Asatryan and A. A. Kirakosyan, *Phys. B*, 2007, **389**, 258–262.
7 J. S. Bhat, R. A. Nesargi and B. G. Mulimani, *J. Appl. Phys.*, 2009, **106**, 033701.
8 B. K. Ridley, *Rep. Prog. Phys.*, 1991, **54**, 169.
9 T. C. Phong, L. N. Minh and N. D. Hien, *Nanoscale Adv.*, 2024, **6**, 832–845.
10 N. D. Hien, *RSC Adv.*, 2022, **12**, 22671–22677.
11 H. K. Dan, P. T. Vinh and N. D. Hien, *Nanoscale Adv.*, 2024, **6**, 6253–6264.
12 L. T. Huong, T. C. Phong, L. N. Minh and N. D. Hien, *Vacuum*, 2024, **220**, 112807.
13 H. T. P. Thuy and N. D. Hien, *Opt Laser. Technol.*, 2025, **182**, 112213.
14 N. D. Hien, *J. Phys. Chem. Solids*, 2022, **161**, 110456.
15 Y. Gu, Y. s. Liu, G. Yang, F. Xie, C. Zhu, Y. Yu, X. Zhang, N. Lu, Y. Wang and G. Chen, *Nanoscale Adv.*, 2021, **3**, 2649–2656.
16 C. X. Ren, *Mater. Sci. Technol.*, 2016, **32**, 418–433.
17 H. Morkoc, *Handbook of Nitride Semiconductors and Devices*, Wiley-VCH, Berlin, 2008.
18 S. Nakamura and M. R. Krames, *Proc. IEEE*, 2013, **101**, 2211–2220.
19 S. Chowdhury and U. K. Mishra, *IEEE Trans. Electron Devices*, 2013, **60**, 3060–3066.
20 D. Wickramaratne, J.-X. Shen, C. E. Dreyer, A. Alkauskas and C. G. Van de Walle, *Phys. Rev. B*, 2019, **99**, 205202.
21 J. B. Varley, A. Janotti and C. G. Van de Walle, *Phys. Rev. B*, 2016, **93**, 161201.
22 M. S. Shur and M. A. Khan, *MRS Bull.*, 1997, **22**, 44–50.
23 B. E. Foutz, S. K. O'Leary, M. S. Shur and L. F. Eastman, *J. Appl. Phys.*, 1999, **85**, 7727–7734.
24 J. Ruch, *IEEE Trans. Electron Devices*, 1972, **19**, 652–654.
25 H. T. P. Thuy, *Micro Nanostruct.*, 2025, **198**, 208059.
26 N. D. Hien, L. Dinh and N. T. Tuyet Anh, *J. Phys. Chem. Solids*, 2020, **145**, 109501.
27 H. Reinen, T. Berendschot, R. Kappert and H. Bluyssen, *Solid State Commun.*, 1988, **65**, 1495–1499.
28 N. L. Kang, *Jpn. J. Appl. Phys.*, 2016, **55**, 035201.
29 H. B. Teng, J. P. Sun, G. I. Haddad, M. A. Stroscio, S. Yu and K. W. Kim, *J. Appl. Phys.*, 1998, **84**, 2155–2164.
30 E. P. Pokatilov, D. L. Nika and A. A. Balandin, *J. Appl. Phys.*, 2004, **95**, 5626–5632.
31 K. Huang and B. Zhu, *Phys. Rev. B: Condens. Matter Mater. Phys.*, 1988, **38**, 13377–13386.
32 M. C. Tatham, J. F. Ryan and C. T. Foxon, *Phys. Rev. Lett.*, 1989, **63**, 1637–1640.
33 A. Seilmeier, H.-J. Hübner, G. Abstreiter, G. Weimann and W. Schlapp, *Phys. Rev. Lett.*, 1987, **59**, 1345–1348.
34 T. Ruf, K. Wald, P. Y. Yu, K. Tsen, H. Morkoç and K. Chan, *Superlattices Microstruct.*, 1993, **13**, 203.
35 G. Weber, A. de Paula and J. F Ryan, *Semicond. Sci. Technol.*, 1991, **6**, 397–400.
36 M. Kisin, V. Gorfinkel, M. Stroscio, G. Belenky and S. Luryi, *J. Appl. Phys.*, 1997, **82**, 2031–2038.
37 K. Huang and B.-F. Zhu, *Phys. Rev. B: Condens. Matter Mater. Phys.*, 1988, **38**, 2183–2186.

38 C.-J. Zhang and K.-X. Guo, *Jpn. J. Appl. Phys.*, 2007, **39**, 103–108.
39 L. T. T. Phuong, L. Dinh and N. D. Hien, *J. Phys. Chem. Solids*, 2020, **136**, 109127.
40 N. D. Hien, *Jpn. J. Appl. Phys.*, 2019, **114**, 113608.
41 N. D. Hien, *Phys. Scr.*, 2023, **98**, 065940.
42 H. K. Dan, L. Dinh, H. D. Trien, T. C. Phong and N. D. Hien, *Jpn. J. Appl. Phys.*, 2020, **120**, 114043.
43 J. S. Bhat, B. G. Mulimani and S. S. Kubakaddi, *Phys. Rev. B: Condens. Matter Mater. Phys.*, 1994, **49**, 16459–16466.
44 H. T. Phuong Thuy and N. D. Hien, *Nanoscale Adv.*, 2025, **7**, 1989–2002.
45 S. Rudin and T. L. Reinecke, *Phys. Rev. B: Condens. Matter Mater. Phys.*, 1990, **41**, 7713–7717.
46 J. S. Bhat, B. G. Mulimani and S. S. Kubakaddi, *Phys. Status Solidi B*, 1994, **182**, 119–131.
47 I. S. Gradshteyn and I. M. Ryzhik, *Table of Integrals, Series, and Products*, Elsevier, California, 8th edn, 2007.
48 R. Zheng, T. Taguchi and M. Matsuura, *Phys. Rev. B: Condens. Matter Mater. Phys.*, 2002, **66**, 075327.
49 J.-j. Shi, *Phys. Rev. B: Condens. Matter Mater. Phys.*, 2003, **68**, 165335.
50 H. Harima, *J. Phys.: Condens. Matter*, 2002, **14**, R967.
51 S. Strite and H. Morkoç, *J. Vac. Sci. Technol., B: Microelectron. Nanometer Struct.-Process., Meas., Phenom.*, 1992, **10**, 1237–1266.
52 M. Masale and N. C. Constantinou, *Phys. Rev. B: Condens. Matter Mater. Phys.*, 1993, **48**, 11128–11134.
53 C. G. Rodrigues and R. Luzzi, *Pramana-J. Phys.*, 2021, **95**, 7053.
54 V. Gruzinskis, P. Shiktorov, E. Starikov and J. H. Zhao, *Semicond. Sci. Technol.*, 2001, **16**, 798.
55 S. Ardali, E. Tiras, M. Gunes, N. Balkan, A. O. Ajagunna, E. Iliopoulos and A. Georgakilas, *Phys. Status Solidi C*, 2011, **8**, 1620–1624.
56 J. Gong, X. X. Liang and S. L. Ban, *J. Appl. Phys.*, 2006, **100**, 023707.
57 K. Schwab, E. A. Henriksen, J. M. Worlock and M. L. Roukes, *Nature*, 2000, **404**, 974–977.
58 T. S. Tighe, J. M. Worlock and M. L. Roukes, *Appl. Phys. Lett.*, 1997, **70**, 2687–2689.